frontiers | Frontiers in Environmental Science

TYPE Review
PUBLISHED 20 February 2023
DOI 10.3389/fenvs.2023.1104320

OPEN ACCESS

EDITED BY
Jing Han,
Institute of Microbiology (CAS), China

REVIEWED BY
Virendra Kumar Yadav,
Mody University of Science and Technology, India
Sedky Hassan,
Sultan Qaboos University, Oman

*CORRESPONDENCE
Mayuri Chabukdhara,
mayuri.chabukdhara@cottonuniversity.ac.in
Tabarak Malik,
malikitrc@gmail.com

†These authors have contributed equally to this work

SPECIALTY SECTION
This article was submitted to Water and Wastewater Management, a section of the journal Frontiers in Environmental Science

RECEIVED 21 November 2022
ACCEPTED 30 January 2023
PUBLISHED 20 February 2023

CITATION
Boruah H, Tyagi N, Gupta SK, Chabukdhara M and Malik T (2023), Understanding the adsorption of iron oxide nanomaterials in magnetite and bimetallic form for the removal of arsenic from water.
Front. Environ. Sci. 11:1104320.
doi: 10.3389/fenvs.2023.1104320

Understanding the adsorption of iron oxide nanomaterials in magnetite and bimetallic form for the removal of arsenic from water

Himangshu Boruah[1†], Neha Tyagi[2†], Sanjay Kumar Gupta[2], Mayuri Chabukdhara[1*] and Tabarak Malik[3*]

[1]Department of Environmental Biology and Wildlife Sciences, Cotton University, Guwahati, India, [2]Department of Civil Engineering, Indian Institute of Technology Delhi, Hauz Khas, India, [3]Department of Biomedical Sciences, Institute of Health, Jimma University, Jimma, Ethiopia

Arsenic decontamination is a major worldwide concern as prolonged exposure to arsenic (>10 μg L^{-1}) through drinking water causes serious health hazards in human beings. The selection of significant, cost-effective, and affordable processes for arsenic removal is the need of the hour. For the last decades, iron-oxide nanomaterials (either in the magnetite or bimetallic form) based adsorptive process gained attention owing to their high arsenic removal efficiency and high regenerative capacity as well as low yield of harmful by-products. In the current state-of-the-art, a comprehensive literature review was conducted focused on the applicability of iron-based nanomaterials for arsenic removal by considering three main factors: (a) compilation of arsenic removal efficiency, (b) identifying factors that are majorly affecting the process of arsenic adsorption and needs further investigation, and (c) regeneration capacity of adsorbents without affecting the removal process. The results revealed that magnetite and bimetallic nanomaterials are more effective for removing Arsenic (III) and Arsenic (V). Further, magnetite-based nanomaterials could be used up to five to six reuse cycles, whereas this value varied from three to six reuse cycles for bimetallic ones. However, most of the literature was based on laboratory findings using decided protocols and sophisticated instruments. It cannot be replicated under natural aquatic settings in the occurrence of organic contents, fluctuating pH and temperature, and interfering compounds. The primary rationale behind this study is to provide a comparative picture of arsenic removal through different iron-oxide nanomaterials (last twelve yearsof published literature) and insights into future research directions.

KEYWORDS

arsenic removal, adsorption, magnetite nanoparticles, isotherms, bimetallic iron oxide nanoparticles, regenration

1 Introduction

The United Nations General assembly (2010) report states that access to safe drinking water and sanitation is a human right. Rapid urbanization and industrialization polluted the majority of the water resources. Major pollutants are organic compounds, dyes, heavy metals (Pb, As, Hg, Cu, Fe, Ni, Pd, *etc.*), agricultural and industrial wastes, recalcitrant compounds, and spills (Lin et al., 2022; Moreira et al., 2021; Zamora-Ledezma et al., 2021; Moosavi et al., 2020; Qi et al., 2023; Bhardwaj et al., 2022.). It was noted that prolonged consumption of

arsenic-containing water could lead to severe health conditions in humans, including arsenicosis, cardiovascular disease, diabetes, and cancer. (Rahaman et al., 2021; Shokoohi et al., 2021).

Arsenic exposure during pregnancy and early childhood can impair cognitive development in young adults (Tyler et al., 2014). Recently published literature revealed that approximately 230 million people from 108 screened countries, majorly from India, Bangladesh, Nepal, Vietnam, China, United States, and Canada, are affected by the elevated concentration levels of arsenic in groundwater set by the World Health Organization (WHO, maximum permissible limit = 10 μg L-1) (Shaji et al., 2021). Geogenic arsenic contamination accounts for over 90% of all arsenic pollution (Shaji et al., 2021). Arsenite or As(III) is most lethal and highly mobile among arsenate or As(V) (60 times) and methylated arsenic compounds (70 times) (De et al., 2009). Moreover, the uncharged nature of As(III) species over a wide pH range makes it's comparably very challenging to get rid of it in water as compared to As(V) (Qi et al., 2015). Rigorous efforts have been made to eliminate arsenic from contaminated water using conventional and novel technologies worldwide. Out of these, adsorption gained attention due to its flexible design systems, cost-effectiveness, and simple operating steps (Jaspal et al., 2020; Liu et al., 2020; Supplementary Figure S1). Also, researchers and scientists have reported different metal-based adsorbents (Fe, Ti, Zr, Cu, and Ce) for arsenic removal (McDonald et al., 2015; Sakthivel et al., 2017; Wen et al., 2019; Nazari et al., 2020; Peng et al., 2022). Out of these, Iron-based nanomaterials (nanoscale zerovalent iron, maghemite, and magnetite based NPs) and their functional derivatives exhibit excellent affinity towards water dissolved arsenic compounds (Bangari et al., 2020); and, are biocompatible and induced less/no toxic effect in various cell lines, plants and vital organs of different animal models (Iannone et al., 2016; Nguyen et al., 2020). Furthermore, a bimetallic sequence of nanosized iron with copper (Fe–Cu), cerium (Fe–Ce), manganese (Fe-Mn), titanium (Fe–Ti), and zirconium (Fe-Zr) can effectively be lowering the arsenic contamination in polluted water (Zhang et al., 2013; Wen et al., 2019; Sha et al., 2020; Rao et al., 2015; Ren et al., 2011). This study aims to do a detailed and comprehensive literature search on the removal of As from the water environment and analyze the last 12 years' research articles (review and original work), book chapters, and conference proceedings. This state-of-the-art focuses on iron-based nanomaterials' uses for water's arsenic removal using iron-based nanomaterials and nanoparticles and bimetallic systems. The objective is to (i) compile information regarding well-addressed iron-based nanomaterials for arsenic adsorption (ii) identify factors that are majorly affecting the process of arsenic adsorption and need further investigation (iii) discuss the separation of arsenic laden exhausted adsorbents and their regeneration capability, (iv) provide brief insights on toxicity and biocompatibility of iron-based nanomaterials and (v) summarize and identified key issues (future directions).

2 Research methodology

An in-depth study was conducted on several peer-reviewed journal papers (research articles and reviews) from several recognized databases (e.g., Sciencedirect, Hindawi publishing corporation, MDPI, Springer, Wiley, Taylor and Francis, ACS publications, and Royal Society of Chemistry) mostly from 2010 to 2021. Additional sources such as book chapters, conference proceedings, and technical journals were also referred to improve the quality of the presented study. The following search expressions were mainly used in search engine: "Iron supported magnetic nanoparticles" OR "Biocompatibility" OR "Iron supported arsenic adsorption" OR "Conjugation" OR "Adsorption" OR "Density functional theory" OR "Magnetite nanoparticles" OR "Desorption" OR "Nano iron (II) aluminum (III) oxide" OR "Biochar" OR "Magnetic composite" OR "Nanofibre filter" OR "Thermodynamics and kinetics parameters" OR "Film diffusion mechanism" OR "Exothermic" OR "Endothermic" OR "Adsorption isotherms models" OR "Langmuir isotherms" OR "Freundlich isotherm" or "Adsorption characteristics" OR "Bimetallic systems" OR "Thermal decomposition" OR "Co-precipitation" OR "Fe_3O_4 nanoparticles embedded anodic aluminum oxide membrane "OR "Magnetic iron oxide-carbon nanocomposites" OR "Magnetite–silica nanocomposites" OR "Maghemite (γ-Fe_2O_3) modified with Fe-Mn binary oxide" OR "Fe–Mn binary oxide incorporated magnetic graphene oxide" OR "Fe-Mn modified biochar composite" OR "Regeneration" OR "Nanosheet iron" OR "Regeneration of spent adsorbents". Mendeley software was used to compile and analyze the collected material as per the organization of the review and requirement. Firstly, selected journal papers were collected and categorized by exploring the above-stated keywords in the journal title, keywords, and abstract. Secondly, duplicate papers were eliminated. Lastly, papers of particular interest were gathered according to the various categories for further review, and document preparation (Figure 1) shows the overall strategy adapted to preparing the current state-of-the-art).

3 Arsenic removal by adsorptive processes

Arsenic removal from water has been reported using a variety of adsorption processes and mechanisms (primarily based on intermolecular interactions). Such as surface complexation reactions or ion/ligand exchange, electrostatic interactions, Lewis acid-base interaction, filling up of size-specific pores present in the adsorbents, and oxidation of As(III) into As(V) before adsorption (Figure 2) (Stumm, 1992; Singh et al., 2020; Wang et al., 2020; Wen et al., 2020). Mainly, arsenic removal from water involves both physisorption and chemisorption processes. In water, the surface of metal oxide adsorbents is covered by many hydroxyl groups due to the dissociative chemisorption of water molecules or the chemical composition of the adsorbent (Wang et al., 2020). On the other side, anionic arsenic species (solute ligand) also contain identical hydroxyl groups, which could replace the surface hydroxyl group present on the adsorbent surface through coordinative ligand exchange to form ligand surface complexes/inner-sphere complexes (Figure 2A) (Stumm, 1992). Surface charges on the adsorbent change with the pH of the solution. At pH levels below point zero charge (pHpzc), adsorbent surfaces are positively charged due to a protonation reaction. Further, the adsorption of OH^- above the pHpzc value turns the adsorbent surface negative (Bangari et al., 2019). In

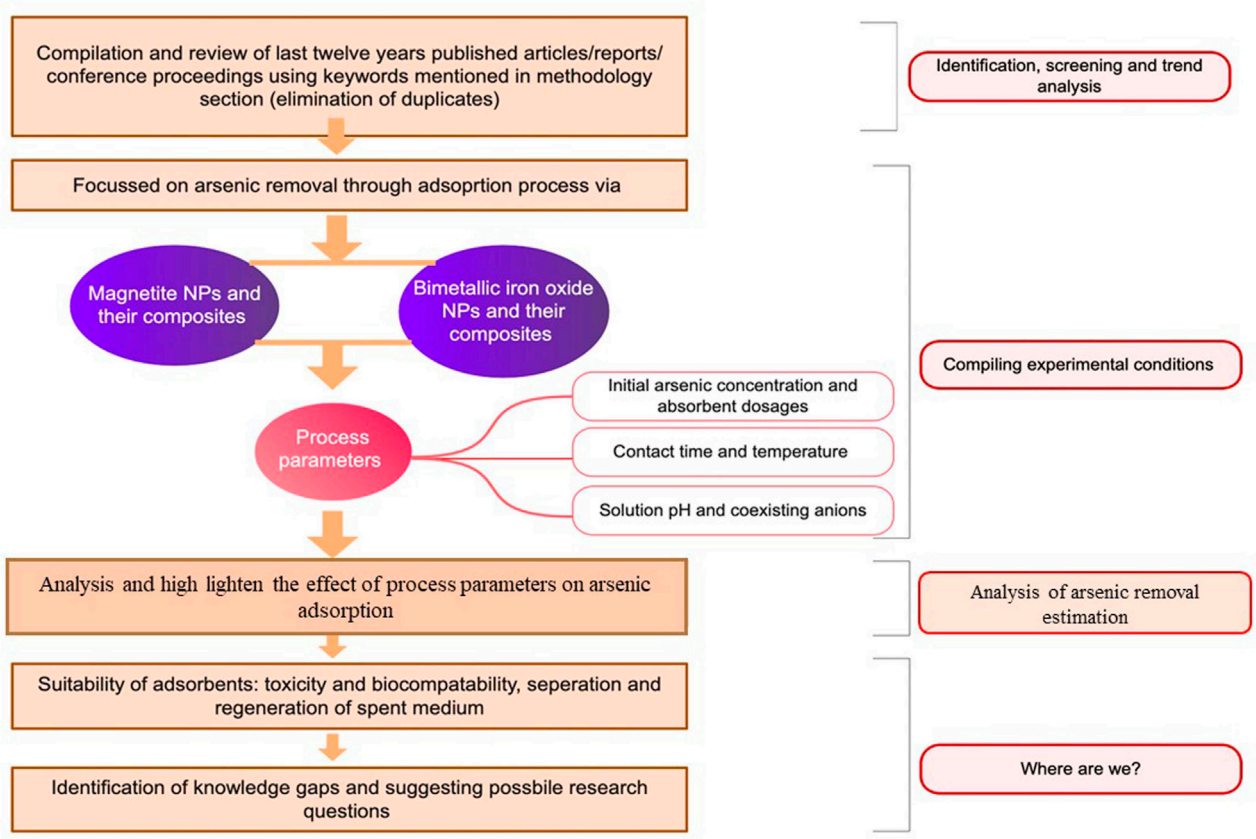

FIGURE 1
Roadmap used for the presented study.

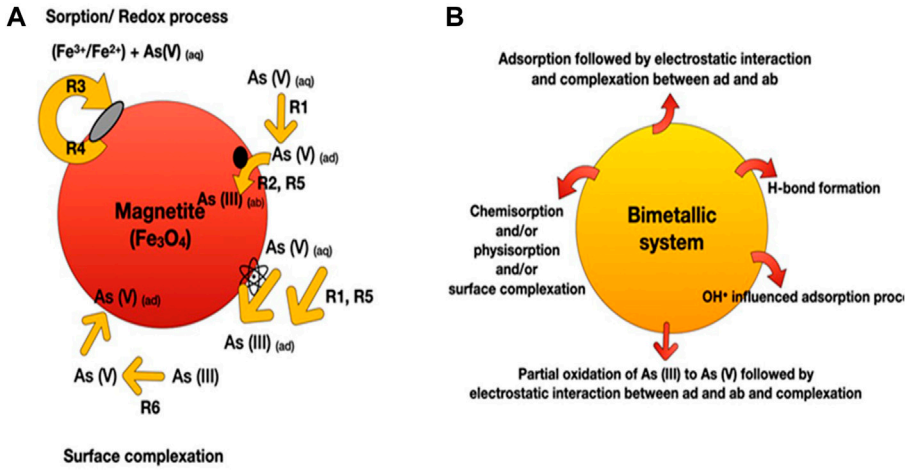

FIGURE 2
Pictorial representation shows the various mechanism involved in the adsorption process of arsenic using **(A)** magnetite NPs and **(B)** bimetallic iron oxide nanomaterials (where iron is coupled with metals oxides and or graphene oxides). Depending upon the iron nanomaterials, arsenic can be removed by R1 = adsorption, R2 = absorption, R3 = precipitation, R4 = dissolution, R5 = reduction, R6 = oxidation, or a combination of these. Finally, surface complexation was formed as an end step. As = arsenic, ad = adsorbent, ab = absorbent, aq = aqueous.

TABLE 1 Removal of arsenic by magnetite nanoparticle based adsorbents.

Adsorbent characteristics	Adsorption characteristics		Separation and Regeneration	Process parameter	Reference
	As(III)	As(V)			
Magnetite nanoparticles (Fe_3O_4, Mn, Zn, Co-doped Fe_3O_4) Thermal decomposition; 8.50 (PS); 80 (Ms); ~5 (pHPZC)	SO; LIM; 653.7, 678.5, 714.7, 629.1 for Fe_3O_4, Mn, Zn, Co-doped Fe_3O_4 respectively (q_m); 24 (t_{eq})		NaOH (0.1M); 4 (RC); 274 ± 22 (q_m for undoped Fe_3O_4)	[As]=1-750; [Ads]=0.6; pH=10; T=25	Pardo et al. (2021)
Superparamagnetic iron oxide nanoparticles (SPIONs) confined Polyvinyl alcohol (PVA) nanofiber membrane Coprecipitation; 9.0 ± 2.1 (PS); 70-80 (dM); 1.4 (ρA); 74 (Ms)		LIM; 52 ± 5 (q_m); 6 (t_{eq})		[As]=0.25-1.5; [Ads]=0.0084; pH =3; T=25	Torasso et al. (2021)
Magnetic composite based on eucalyptus wood biochar (MEWC) 61 ± 20(PS);73(S);0.12(Vp); 11.2Am^2 kg^{-1} (Ms)		21.45 (q_m)	Magnetic	[As]=0.1; [Ads]=5; pH=7; T=25; For natural water η= 72% for [As]= 0.107; η=80% for [As]= 0.079	Bursztyn Fuentes et al. (2021)
Polyaniline Microsphere/Fe_3O_4 nanocomposite ~10 (PS); ~64 (S); 9.897–10.561(D); 0.16–0.17(Vp); ~24.39 (Ms); 7.7 (pHPZC)	PSO; FIM; 28.27 (q_m); 4 (t_{eq})	PSO; FIM; 83.08 (q_m); 4 (t_{eq})	NaOH (0.1M and 0.5 M);3 (RC); 83 (η_R)	[As(III)]=0.1-1000; [Ads]=1; pH =~7; T=~27; $\eta(PO_4^{3-})$=59; $\eta(CO_3^{2-})$=63	Dutta et al. (2020)
Hybrid Iron Oxide-Biochar Nanocomposite (RHIOB and WHIOB) Proprietary copyrolysis; 2-20 (PS); For RHIOB: 300.0 (S); 18.07 (Vp); 0.012 (D); 5.5(pHpzc) For WHIOB: 339.0 (S); 18.72 (Vp); 0.014 (D); 7.0(pHpzc)	Endothermic; PSO; 12 (t_{eq}); Redlich–Peterson; 0.096 (q_m) for RHIOB; Sips, Koble-Corrigan;0.111 (q_m) for WHIOB		NaOH(0.1 N) and NaCl(0.1 N); 4 (RC); 86 (η_RRHIOB); 90 (η_RWHIOB)	[As(III)]=0.05-1; [Ads]=2.0; pH =6.5 and 7.5; T=10, 25, 40; $\eta(PO_4^{3-})$=~20(RHIOB) and~30(WHIOB)	Singh et al. (2020)
Lcysteine-functionalized mesoporous magnetite nanosphere Solvothermal and post-treatment; 150-200(PS); 66.5 (S); 3.9 (D); 42.50 (Ms); 5.10 (pHPZC)	Endothermic; PSO; LIM; 20 (q_m); 2 (t_{eq})	Endothermic; PSO; LIM; 34 (q_m); 1.5 (t_{eq})	Magnetic; NaOH (0.1 M); 5 (RC); 65 for As(III) and 70 for As(V) (η_R)	[As]=1-40;[Ads]=0.08 for As(III) and 0.06 for As(V); pH=7 for As(III) and 5 for As(V); T=25; $\Delta\eta(PO_4^{3-})$=~40 for As(III), ~50 for As(V)	Tripathy et al. (2020)
Fe_3O_4-functionalized boron nitride nanosheets 179.5(S); 3.25(D); 0.1459 47.39 (Ms); 2.1 (pHPZC)	Endothermic; LIM; PSO; 30.3 (q_m); 8(t_{eq}); 134 and 556 ppb of As(III) in real water samples were reduced to 2.67 and 10.29 ppb at 25 °C and 35 °C respectively.		NaOH(1.0M); 5(RC); Unaltered adsorption capacity	[As]= 6-70; [Ads]=0.4, pH=8; T=25	Bangari et al. (2020)
1-butyl-3-methylimidazolium hexafluorophosphate ([BMIM][PF6])-modified magnetic graphene oxide(MGO-IL) 79 (dL); 27.79 (Ms)	Endothermic; LIM; PSO; 160.65 (q_m); 0.5(t_{eq})	Endothermic; FIM; PSO; 104.125 (q_m); 0.5(t_{eq})	HCl (0.1 M); 5(RC); 8.06 for (As III) and 14.14 for (AsV) (Δη)	[As]=20-250; pH=7; T=45; qm(PO_4^{3-})=~40 (AsIII); qm(PO_4^{3-})= ~25 (AsV)	Zhang et al. (2019)
Magnetite immobilized on pine cone Base washing and Co-precipitation; 37.50 (Ms); 4.26 (pHPZC of MNP-PCP-AsIII)	PSO; LIM; 18.02 (q_m); 0.5(t_{eq})		Filtration or magnetic; NaOH and HCl (0.1 mg.dm-3); 5(RC); 11.17 (q_m)	[As]=25-150φ; [Ads]=5φφ; pH=8; T=26; $q_m(PO_4^{3-})$=5.67	Pholosi et al. (2019)

(Continued on following page)

TABLE 1 (*Continued*) Removal of arsenic by magnetite nanoparticle based adsorbents.

Adsorbent characteristics	Adsorption characteristics		Separation and Regeneration	Process parameter	Reference
	As(III)	As(V)			
Fe_3O_4 nanopaeticles embedded anodic aluminum oxide membrane Anodization and ultrasonication; 35–45(PS); 19.826 (S);7.2126(D); 0.0357 (Vp); 7.2(pHPZC)		Endothermic; PFO; LIM; 83.3 (q_m); 0.67 (t_{eq}); 84.2-94.5 (η) for real water		[As]=0-0.35; pH=6; T=25; $\eta(PO_4^{3-})$=~20; $\eta(SO_4^{3-})$=~30;	Maghsodi and Adlnasab (2019)
Fe_3O_4@TA@UiO-66 microsphere Co-precipitation and in-situ crystal growth; 200 ± 10 (PS); 130.3 (S); 4 (D); 0.18 (Vp); 3 (pHPZC)	PSO; LIM; 97.8 (q_m); 24 (t_{eq})			[As]=0.5-40; [Ads]=0.2; pH=3-11; T =25; Insignificant impact of PO_4^{3-}, SO_4^{2-}, CO_3^{2-}, SiO_3^{2-}	Qi et al. (2019)
Polyethersulfone membranes impregnated with (3aminopropyltriethoxysilane) APTES-Fe_3O_4 nanoparticles Phase inversion; 12.15 (Mean Pore radius); 0.71 Porosity (%)		FIM; 14.6 (q_m); 4.5(t_{eq})		[As]=2-8; [Ads]=0.5; pH=2; T=25	Rowley and Abu-Zahra (2019)
Magnetite microparticles decorated cellulose sponge Co-precipitation;~14.2(PS); 4.08 (Ms); 7.2 (IEP)		PSO; LIM; 349.9 (q_m); 1(t_{eq})	NaOH; 5 (RC); 82 (η_R)	[As(V)]=50-250; [Ads]=0.018; pH=7; qm(SO_3^{2-})=111.1; qm(NO_3^-)=130; qm(F-) =133.3	Nagarajan and Venkatanarasimhan (2019)
Magnetite-Coated Boron Nitride Nanosheets Bottom up; 10-22 (PS);119.1 (S); 17.41 (D); 0.355 (Vp); 49.19 (Ms); 2.86 (pHPZC)		Endothermic for 10-30°C; Exothermic beyond 30°C; LIM; PSO; 26.3 (q_m); 10 (t_{eq})	Magnetic; NaOH (1.0 M)	[As(V)]=50; [Ads]=0.4; pH=2.0; T=~25	Bangari et al. (2019)
TiO_2 nanoparticles anchored on Fe_3O_4 magnetic nanosheets Sol-gel, hydrothermal assisted crystallization;89.4 (S); 0.186 (Vp); 8 (D); 6.8 (pHPZC); ~20.0 (Ms)	PSO; LIM; 30.96 (q_m); 0.75 (t_{eq})	PSO; LIM; 36.36 (q_m); 0.75 (t_{eq})	Magnetic; NaOH (0.1 M); 5(RC); 60 (η_R)	[As]= 0-50; [Ads]= 0.32; pH=7; UV-assisted removal of As(III); $\eta(SiO_3^{2-})$, $\eta(HPO_4^{2-})$ was ~30 for As(V) and ~20 for As(III)	Deng et al. (2019)
Fe_3O_4 blended Polyethersulfone (PES) membrane 20(PS); 31.9 (S); 6.8-30.3 (D); 0.057(Vp)		325.8 (q_m) (Recirculating filtration);147.9 (q_m) (static adsorption)	NaOH (0.05 M); 2(RC); 92.7 (R)	[As]=20-100; [Ads]=0.1; pH=7; T= 25	Zhang et al. (2018)
Yttrium-doped Iron oxide Precipitation; 10(PS); 7.0 (pHPZC)	PSO; FIM; 84.22 (q_m); 4(t_{eq})	PSO; FIM; 170.48 (q_m); 24 (t_{eq})	Magnetic; NaOH (0.5-M); 3(RC); 52.7 for As(III) and 64.0 for As(V) (η_R)	[As]= 1- 100; [Ads]=0.1; pH=7.0; T=25; $\eta(PO_4^{3-})$=~42.4 for (AsIII) and 64.1for (AsV)	Yu et al. (2018)
Magnetic iron oxide-carbon nanocomposites Coprecipitation and hydrothermal; 20 (PS); 35.1 (Ms)		PSO; LIM; 20.05 (q_m); 2.5(t_{eq})	Magnetic	[As]=10-50; [Ads]=0.02; pH=1-2; T=25	Huong et al. (2018)
Iron supported on bioinspired green silica 244 (S); 18.6 (D);0.75 (Vp)		LIM; FIM; 69.64 (q_m); 2 (t_{eq})	NaOH (0.1 M); 6 (RC); ~100(η_R)	[As]=40-100φφφ; [Ads]=0.5; pH=3; T=20	Alotaibi et al. (2017)

(Continued on following page)

TABLE 1 (*Continued*) Removal of arsenic by magnetite nanoparticle based adsorbents.

Adsorbent characteristics	Adsorption characteristics		Separation and Regeneration	Process parameter	Reference
	As(III)	As(V)			
Iron oxide–graphene oxide nanocomposite Co-precipitation; 5 (PS); 341(S); 0.29 (Vp); 7 (D); 5.9 (pHPZC)	PSO; LIM; 147 (q_m); 70% in15 min	PSO; LIM; 113 (q_m); 77% in 15 min	Filtration	[As]=0.1–1200; pH=7 for As(III), 3As(V); [Ads]=0.8; T=23; PO_4^{3-}, reduced arsenic adsorption	Su et al. (2017a)
Carbon nanosphere–iron oxide nanocomposites Catalytic emulsion polymerization and surface oxidation; 3–4 (PSFeOx); 311 (S); 24 (D); 0.55(Vp); 2.8 (pHPZC)	PSO; FIM; 416 (q_m); 62 % in 30 min (η)	PSO; FIM; 201 (q_m); 73% in 30 min (η)	Filtration	[As]=50–2000; [Ads]=1; pH=8 for As(III) and 3 for As(V); T=23	Su et al. (2017b)
Magnetic sludge composite Co-precipitation; 2-25(PS); 78 (S); 0.53 (Vp); 44(D); 7(pHPZC); 52.2 (Ms)		PSO; LIM; 18.5(q_m); 5 (t_{eq})	Magnetic	[As(V)]=0.1-5; [Ads]=0.7; pH=2.6; T=25; qm(PO_4^{3-})= ~5	Wang et al. (2016)
Yeast cross-linked Fe_3O_4 nanoparticles Nano-precipitation; <50 (PS); 52 (Ms); 43.6 (S); 0.089 (Vp)		PSO; LIM; 28.70 (q_m); 3(t_{eq})	Magnetic; HCl or NaOH (0.1M); 40 (γ)	[As(V)]=0.5-2.5; [Ads]=1-4; pH= 7.5; T=30	Rajesh Kumar et al. (2016)
Superparamagnetic iron oxide nanoparticle (SPION) loaded polyacrylonitrile nanofibers (HPAN) 10.2(PS_{SPION}); 80 (Ms); 465 ± 39 (PS_{HPAN})		Batch mode: 32.5* (q_m) Continuous flow mode:851.7 (q_m)		[As(V)]=100;[Ads]=0.1; pH=3.8-4.0	(Morillo et al., 2016) *
Humic acid coated graphene in the Fe_3O_4 nano-composite Co-precipitation; 8 (PS); 0.7883 - 0.9060 (S); 2-50 (D)	LIM; 8.67 (q_m); 24 (t_{eq})	LIM; 61.73 (q_m); 24 (t_{eq})	Magnetic	[As]=1-10; [Ads]=0.2; pH = 7.0; T=23	Paul et al. (2015)
Forager Sponge-loaded superparamagnetic iron oxide Coprecipitation and surface immobilization; 10.2 (PS); 30 (Ms)	LIM; 2.1* (q_m); 1 (t_{eq})	LIM; 12.1* (q_m); 1 (t_{eq})	Centrifugation; HNO_3 (1.0 M); 97.2 (R or γ)	[As]=1-1000; [Ads]=0.05; pH=3.8; T=23; Δη PO_4^{3-} = 88.8; Δη(PO_4^{3-}, CI^-, NO_3^{2-}, SO_4^{2-})=85.9 for As(V)	(Morillo et al., 2015a) *
3-mercaptopropanoic acid-coated superparamagnetic iron oxide nanoparticles Coprecipitation, surface coating; 15–20 (PS)		LIM; 2* (q_m); 1(t_{eq})	HNO_3 (1.0 M) and NaCl (1.0 M); 97 for HNO_3 and 5 for NaCl (R)	[As]=1.3×105 -1.3×102**; pH=4; T=23; Δη(PO_4^{3-}) = 94.9; Δη(NO_3^{2-}) = 86.6; Δη(SO_4^{2-}) = 56.9; Δη(CI^-) = 44.8	(Morillo et al., 2015b) *
Magnetite–silica nanocomposites Co-precipitation; 29 (PS); 163.54 (S); 8.69 (pHPZC)		170*** (q_m)	Magnetic	[As]=~0.3-1.2; [Ads]=0.1; pH=6; T =25	Kokate et al. (2013)
Fe_3O_4/SiO_2 core–shell nanorods Coprecipitation;10–30(PS); 335.72 (S); 9.1791 (D); 0.6933(Vp); 21.24 (Ms)	PSO; LIM; 16.58 (q_m); 5min (t_{eq})	PSO; LIM; 46.01(q_m); 5min (t_{eq})	Magnetic; HCl (0.1 M); 3(RC); ~10(Δη)	[As]=3-7; [Ads]=0.2; pH=7; T=30	Babu et al. (2013)

(Continued on following page)

TABLE 1 (*Continued*) Removal of arsenic by magnetite nanoparticle based adsorbents.

Adsorbent characteristics	Adsorption characteristics		Separation and Regeneration	Process parameter	Reference
	As(III)	As(V)			
Spherical polystyrene-supported nano-Fe_3O_4 Hetero-coacervation; 20–30 (PS); 350–400 (PSpolystyrene beads)		PFO; LIM; 139.3 (q_m); ~0.83 (t_{eq})	Magnetic; NaOH (0.1 M); 6 (RC); 93.8 (η_R)	[As(V)]=1-50; [Ads]=0.5; pH=6.0; T=25; PO_4^{3-}, SiO_3^{2-} inhibited arsenic adsorption	Jiang et al. (2012)

PS (Average size of nanoparticles in nm); S (Surface area of nanoparticles in $m^2\ g^{-1}$); D (Average pore size of adsorbent in nm); dL (Lamellar thickness in nm); dM (Membrane thickness in μm); ρA (Mass surface density in mg cm^{-2}); Vp (Pore volume of adsorbent in cm^3g^{-1}); Ms (Saturation magnetization of adsorbent in emu g^{-1}); pH_{PZC} (Point Zero Charge of adsorbent); IEP (Isoelectric point); As(III), As(V) (Contaminant arsenic species); [As(III)] and [As(V)] (Initial arsenic concentration in mg L^{-1}); [Ads] (Adsorbent dose in gL^{-1}); T (Temperature °C); t_{eq} (Equilibrium time in Hour (h)); η (Efficiency in %); Δη (Reduction of removal efficiency in %); q_m (Maximum adsorption capacity in mg g^{-1}); γ (Desorption efficiency in %); R (Arsenic recovery ratio in %); RC (Number of regeneration cycles); η_R (Residual efficiency after regeneration in %); PFO (Pseudo-First-order); PSO (Pseudo-Second-order); SO (Second-order); LIM (Langmuir isotherm model); FIM (Freundlich isotherm model); RPI (Redlich-Peterson isotherm model); *q_m values were represented in mmol.g^{-1}; **[As] was represented in mol.L^{-1}; *** q_m value was represented in μmol.g^{-1}; ᵠ [As] values were represented in mg.dm^{-3}; ᵠᵠ [Ads] value was represented in g.dm^{-3}; ᵠᵠᵠ [As] values were represented in μg cm^{-3}.

contrast, $FeOH^+$ or $FeOH_2^+$ is the predominant surface group of most iron oxide materials in an acidic environment, while the occurrence of $Fe(OH)_2^0$, FeO^-, $Fe(OH)_3^-$ had been reported in alkaline solutions (Mehta et al., 2015; Wang et al., 2020). In an acidic solution, the protonated surface of metal oxides behaves as weak Lewis acid, which acts as an electron acceptor. Anionic adsorbate species get adhered onto the adsorbent surface either by electrostatic interaction (hard acid-hard base) or by forming covalent complexes (soft acid-soft base) (Wang et al., 2020). For instance, most iron oxide-based adsorbents have point zero charge values in the range five to eight, indicatingthe adsorption of As (V) at lower pH while As(III) at higher pH. Single-step efficient removal of arsenic becomes difficult due to its multivalent character and unequal affinity of different arsenic species toward the surface functional groups of the adsorbents. In well-oxygenated water, As(V) is the primary arsenic species, whereas As(III) is prevalent in groundwater (Ferguson and Gavis, 1972; Smedley and Kinniburgh, 2002). Pre-oxidation of As(III) into As(V) has been proposed in various literature to increase the effectiveness of arsenic removal (Mudzielwana et al., 2019; Sha et al., 2020; Wang et al., 2020). Indeed, the exchange of As(III) to As(V) limits the mobility of arsenic and increases its probability of higher arsenic adsorption efficiency (Lafferty et al., 2010). Several researchers emphasized the use of manganese dioxide (MnO2) for the oxidation of As(III) as a result of its weak oxidation tendency, which is compatible with the specific oxidation of As(III) (Zhang et al., 2017). Moreover, co-occurring oxidation of As(III) to anionic As(V) and further adsorption of As(V) by iron binary oxides (Fe-Mn) leads to superior removal of arsenic with reduced contaminant mobility (Shan and Tong, 2013; Nikić et al., 2021).

3.1 Adsorption based on iron oxide nanomaterials

Fe-based nanomaterials exhibit high surface area, chemical stability, adequate surface distribution of reactive sites, selectivity towards arsenic species, biocompatibility, and notable arsenic adsorption efficiency (Zhang et al., 2019; Nguyen et al., 2020; Nikić et al., 2021). Moreover, facile synthesis methods and efficient magnetic separation of Fe-based nanomaterials from treated water have increased the usability of this class of nanomaterials in arsenic removal processes (Chen et al., 2013a; Deng et al., 2019). Furthermore, as seen in Table 1 and Table 2, promising adsorption capacities of Fe-based nanomaterials after five to six adsorption-regeneration cycles lead to the cost-effective eliminationof arsenic from water (Jiang et al., 2012; Alotaibi et al., 2017).

Different synthesis approaches of Fe-based nanomaterials production include co-precipitation, proprietary copyrolysis, solvothermal, sol-gel, emulsion polymerization, hydrothermal, sonochemical, thermal decomposition and green synthesis methods (Yadav et al., 2020a; Otero-González et al., 2020; Singh et al., 2020; Torasso et al., 2021; Selvaraj et al., 2022). Green synthesis methods of Fe-based nanomaterials are environmentally benign and could be considered as a potential substitute of existing chemical and physical methods due to the affordability, abundance of biomaterials and simple operating procedures (Arslan et al., 2022; Xu et al., 2022). Biomaterials such as plant extracts (eg., green tea), vermicomposting leachate, residual food byproduct (e.g, banana peel) and microorganisms have been explored for synthesis of Fe based nanomaterials by several researcher while another study reported the utilization of incense sticks ash waste as precursor for iron oxide nanoparticle synthesis (Majumder et al., 2019; Yadav et al., 2020b; Chatterjee, et al., 2020; Arslan, et al., 2022; Chen et al., 2022).

3.1.1 Magnetite nanoparticles and their composites

Magnetite (Fe_3O_4) is one of the most studied iron oxides for several environmental remediation processes, including water treatment, due to its high reactivity towards various organic and inorganic pollutants and inherent magnetic properties. The presence of unpaired electrons in Fe^{2+} and Fe^{3+} exerts magnetic sensitivity to the iron oxide nanomaterial-based adsorbents, facilitating their easy separation from water treatment systems (Kokate et al., 2013; Usman et al., 2018). Numerous modifications of iron oxide with different functional groups, alloying with other elements, and researchers and scientists in recent documents have reported incorporation in several organic and inorganic substrates (De et al., 2009; Sha et al., 2020; Singh et al., 2020). Bangari et al. (2019) fabricated magnetite-coated boron nitride nanosheets (BNNS-Fe_3O_4) with a specific surface area of 119 $m^2\ g^{-1}$ and removed ~98.83% of As(V) from arsenic solution *via* exothermic chemisorption process (Figure 3). The rapid increment was observed

TABLE 2 Removal of arsenic by iron bimetallic oxide nanomaterials based adsorbents.

Adsorbent	Adsorption characteristics		Separation and Regeneration	Process parameter	Reference
	As(III)	As(V)			
Fe–Mn binary oxide incorporated magnetic graphene oxide Heterogeneous nucleation, ultrasonication; 20–50 (PS); 219.59 (S); 7.6 (Ms); 4.4 (pH_{PZC})	Exothermic; PSO; LIM and FIM; 24.38 (q_m); 12 (t_{eq})		Magnetic; NaOH (0.5 $molL^{-1}$) and NaClO (0.1 $molL^{-1}$); 5 (RC); 5.1(Δη)	[As]=2–30; [Ads]=0.5; pH=3-10; T=25±2	Sha et al. (2020)
Zirconium and iron oxyhydroxide Hydrothermal method; 49 (S); 8.04 (D); 0.077 (V_p); 7.2 (pH_{PZC})		LIM; 62.7; (q_m); 0.67(t_{eq})		[As]=0.025-10; [Ads]=0.06; pH = 7; T=25; Δq_m(= 81	Vences-Alvarez et al. (2020)
Ordered mesoporous Fe/Ce bimetal oxides Inverse micelle; 118.69 (S); 3.77 (D); 0.265(V_p); 17.4 (Ms); 7.4(pH_{PZC})Inverse micelle; 118.69 (S); 3.77 (D); 0.265(V_p); 17.4 (Ms); 7.4(pH_{PZC})	PSO; LIM; 281.34 (q_m); 1.5 (t_{eq})	PSO; LIM; 216.72; (q_m); 1.5 (t_{eq})	Membrane; NaOH (0.5 M); 6(RC); 95 (η_R)	[As]=1-150; [Ads]=0.2; pH=7; T=25; $\Delta\eta(SiO_3^{2-})$=86.14; $\Delta\eta$ PO_4^{3-} =80.14; ΔHA=68.14 for As(III); $\Delta\eta(SiO_3^{2-})$=79.28; $\Delta\eta$ PO_4^{3-} =67.27; ΔHA= 56.12 for As(V)	Wen et al. (2020)
Maghemite (γ-Fe_2O_3) modified with Fe-Mn binary oxide Co-precipitation; 109 (S); 0.478 (V_p); 8.72 (D); 6.50 (pH_{pzc})	PSO; FIM; 56 (q_m); 9 (t_{eq})	PSO; FIM; 54 (q_m); 9 (t_{eq})	Magnetic; NaCl (0.1 M) + NaOH (0.5 M) + NaOCl (0.01 M); 5 (RC); 18 (Δη AsIII); 12 (Δη AsV)	[As]=0.2-50; [Ads]=0.5; pH=7; T=22±1; PO_4^{3-}, SiO_4^{2-} and CO_3^{2-} reduced arsenic uptake	Nikić et al. (2021)
Fe_2O_3-ZrO_2/BC nanohybrid composite Co-precipitation; 17-22(PS); 8.0 (pH_{pzc})	Endothermic; PSO; FIM; 1.01(q_m)		NaOH(0.2M); 6 (RC); 30 (Δη)	[As(III)]=0.1-1.0; [Ads]=2.0; pH<9; T=27	Siddiqui and Chaudhry (2019)
Fe-Mn Bimetal Modified Kaolin clay 29.8 (S); 8.5 (D)	Exothermic; LIM; PSO; 2.93 (q_m); 1(t_{eq})			[As]=1- 30; [Ads]=4; pH=6.5; T=25	Mudzielwana et al. (2019)
Magnetic mesoporous Fe-Ce bimetal oxides Template nanocasting method; 0.564(V_p); 143.61(S)		PSO; LIM; 111.17 (q_m); 24 (t_{eq})	NaOH (0.1 M); 5 (RC); 90 (η_R)	[As(V)]=1-50; [Ads]=0.2; pH = 3; T=25; Δη (PO_4^{3-}) =28.7; Δη (SiO_3^{2-})=47.9	Wen et al. (2019)
Yttrium-ferric binary composite Co-precipitation; 7(pH_{PZC})		PSO; LIM; 288.7 (q_m); 24 (t_{eq})	Coagulation/sedimentation and filtration	[As]= 1-100; pH=7; [Ads]= 0.1 g/L; T=25; η(PO_4^{3-}) = ~ 100; q_m(F^-)= ~125	Yu et al. (2019)
Iron/copper bimetallic nanoparticles Chemical reduction; 13.17(PS); 79.5 (S); 8-9(pH_{PZC})	PSO; LIM; 19.68 (q_m); 0.5(t_{eq})	PSO; LIM; 21.32 (q_m); 0.25(t_{eq})	Centrifugation, filtration; NaOH(0.1M) 100 for As(V); 70.3 for As(III) (γ)	[As]=0.1-5; [Ads]=0.1; pH =7; T=20 ± 2; Insignificant impact of PO_4^{3-}, SO_4^{2-}, HCO_3^-	Babaee et al. (2018)
Fe-Al bimetallic material 1930.2 (S); 39.49 (D); 0.6(V_p)	Exothermic; PSO; LIM and FIM; 35.34 (q_m); 2 (t_{eq})			[As]=5-500; [Ads]=10; pH =7;T=25	Meng et al. (2018)
Fe-Mn modified biochar composite 208.6 (S); 0.144(V_p); 2.76 (D); 9.80(pH_{pzc})	Endothermic; PSO; FIM and LIM; 8.25 (q_m); 1.25(t_{eq})			[As]=0.2–50; [Ads]=0.01; pH=7; T=25; Δη(PO_4^{3-})=22	Lin et al. (2017)
Porous Nanobimetallic Fe-Mn Cubes ~200 (PS); ~450 (S)	Exothermic; FIM; 460 (q_m)		NaOH (0.1 M); 3(RC); Insignificant reduction in (η_R)	[As]=1-200; [Ads]=0.25; pH=5-9	Zhang et al. (2017)
Ce-Fe bimetal mixed oxide Solvothermal; 290-300 (PS);		PSO; LIM; 32.12 (q_m); 1(t_{eq})	NaOH (0.5 M);4 (RC); 20.15 (q_m)		Sahu et al. (2016)

(Continued on following page)

TABLE 2 (*Continued*) Removal of arsenic by iron bimetallic oxide nanomaterials based adsorbents.

Adsorbent	Adsorption characteristics		Separation and Regeneration	Process parameter	Reference
	As(III)	As(V)			
4.42 (D); 127 (S); 0.185 (V_p); 6.4(IEP)				[As]=1-60; [Ads]=1; pH=3; T=25 ±5; $\eta(CO_3^{2-})$=53; $\eta(PO_4^{3-})$=50	
Fe(III)–Sn(IV) mixed binary oxide-coated sand 38.7(PS); 7.25 (pH_{pzc})	Endothermic; PSO; LIM; 82.64* (q_m); 1(t_{eq})	Endothermic; PSO;LIM; 227*(q_m); 1(t_{eq})	NaOH(0.1 N); 87.5(γ)	[As]= 0.2- 0.8; [Ads]= 8; pH =7; T=20 for As(III), 40 for As(V)	Chaudhry et al. (2016)
Magnetically-Confined Fe-Mn Bimetallic Oxide Hydrothermal; ~200 (PS); 32.0 (S); 18.1 (D); 0.093(V_p); 31.0 (Ms)	LIM and FIM; 56.1 (q_m); 1 (t_{eq})		Magnetic; NaOH (0.2 M); 5(RC); Insignificant decrease in As(III) sorption capacity	[As]=0.5-40; [Ads]=0.25; pH=6.5	Yu et al. (2016)
Iron manganese bimetal oxides 143.88 (S); 5.88/11.52 (D); 0.647(V_p)		FIM; PSO; 35.35(q_m); 24 (t_{eq})	Magnetic; NaOH(1 M); 5 (RC); 9.5(Δη)	[As(V)]=1-50; [Ads]=0.2; pH = 3; T=25	Wen et al. (2015a)
Micro/nano-structured Fe–Ni binary oxides Co-precipitation, calcinations; 3–6 (PS); 245 (S); 3 (D); 0.32(V_p)	PSO; LIM; 168.6 (q_m); 24 (t_{eq})	PSO; LIM; 90.1 (q_m); 24 (t_{eq})	Magnetic	[As]=0.5–1000; [Ads]=0.5; pH= 7; Insignificant impact of SO_4^{2-}, PO_4^{2-} and CO_3^{2-}	Liu et al. (2015b)
Fe–Ti bimetal oxides Co-precipitation; 344.3 (S); 2.51 (D); 5.9–6.2(pH_{PZC})	PSO, two-compartment-FO; FIM; 111.37 (q_m); 24 (t_{eq})	PFO, PSO, two-compartment-FO; FIM; 31.42 (q_m); 24 (t_{eq})	Membrane; NaOH (1 $molL^{-1}$); 3(RC); Δη=26 for As(III) and 12 for As(V)	[As]=0.5–50; [Ads]=0.25; pH =7; Δη(PO_4^{3-})=54 for As(III) and 66 for As(V)	Rao et al. (2015)
Iron cerium bimetal oxides KIT-6 hard template; 134.89 (S); 5.81-11.38 (D); 0.633(V_p); 27.4 (Ms)	PFO; LIM and FIM; 7.29 (q_m); 3 (t_{eq})	PFO; LIM and FIM; 103.36 (q_m); 3 (t_{eq})	Magnetic	[As]=0.1-1; [Ads]= 0.4; pH =3; T=25	Wen et al. (2015b)
Fe–Mn binary oxide impregnated chitosan bead 1.6×10^6-1.8×10^6 (PS); 248 (S); 0.37(V_p)	PSO; FIM; 54.2 (q_m); 36(t_{eq})	PSO; FIM; 39.1 (q_m); 36 (t_{eq})	NaOH(0.5 M); 4(RC); 85 for As(III) and 83 for As(V) (η_R)	[As]=5.4–21.6; [Ads]=1;pH =7; T=25; HPO_4^{2-} reduced arsenic adsorption	Qi et al. (2015)
Fe–Mn binary oxide nanowires Thermal decomposition; 100–500 (PS-Diameter); 57.6 (S); 10.3 (Ms)	PSO; LIM and FIM; 171 (q_m); 1.25 (t_{eq})			[As]=1-15; [Ads]=0.05; pH =7; T=25; $\eta(PO_4^{3-})$=42.5; η(HA)=~87	Cui et al. (2014)
Nanostructured iron(III)-copper(II) binary oxide Co-precipitation; 282 (S); 0.31(V_p); 7.9 (pH_{pzc})	PSO; FIM; 122.3 (q_m); 24 (t_{eq})	PSO; FIM; 82.7 (q_m); 24 (t_{eq})	NaOH(0.5 M); 4 (RC); 10.6(Δη) for As(III); 6.2 for As(V)(Δη)	[As]=5-60; [Ads]=0.2; pH=7.0; $\eta(PO_4^{3-})$= ~40	Zhang et al. (2013)
Nanostructured hollow iron-cerium alkoxides Hydrothermal; ~120 (PS); 217.5 (S); 5.29 (D); 0.262 (V_p)	PSO; FIM; 266.0 (q_m); 4 (t_{eq})	PSO; LIM; 206.6 (q_m); 3(t_{eq})	Membrane	[As]=1- 100; [Ads]=0.2; pH =6; T=25; $\eta(SiO_3^{2-})$=~60 for As(III) and ~40 for As(V); $\eta(PO_4^{3-})$=~40for As(III) and ~30 for As(V)	Chen et al. (2014)
Magnetic nanoscale Fe-Mn binary oxides loaded zeolite Hydrothermal; 20-100 (PS); 340 (S); 50.104 (Ms)	Endothermic; PSO;FIM and R-P IM; 318.25 (q_m); 0.5(t_{eq})	Endothermic; PSO; FIM and R-P IM; 0.5(t_{eq})	Magnetic	[As]= 0.002-0.3; [Ads]=0.5, T=25, pH =7	Kong et al. (2014)
Ce–Fe oxide decorated multiwalled carbon nanotubes Co-precipitation; 7.0 (PS); 216.3 (S); 2.81(D); 1.17(V_p); 4.68 (pH_{PZC})	PSO; LIM; 28.74 (q_m); 5 (t_{eq})	PSO; FIM; 30.96 (q_m); 6 (t_{eq})		[As]=1-20; [Ads]=0.2; pH=4 for As(V) and 7.5 for As(III); T=25	Chen et al. (2013b)

(Continued on following page)

TABLE 2 (*Continued*) Removal of arsenic by iron bimetallic oxide nanomaterials based adsorbents.

Adsorbent	Adsorption characteristics		Separation and Regeneration	Process parameter	Reference
	As(III)	As(V)			
Magnetic nanoparticles modified with Fe-Mn binary oxide Co-precipitation and heterogeneous nucleation; 20-50 (PS); 23.2 (Ms); 6.2 (IEP)	PSO; FIM and Two-site LIM; 47.76 (q_m); 3 (t_{eq})		Magnetic; NaOH(0.5 M)+ NaCl(0.1 M)+ NaClO(0.01 M); 5(RC); ~98(η_R)	[As]=1-15; [Ads]=0.1; pH=7; T=25; $\eta(SiO_3^{2-})$=~50; $\eta(PO_4^{3-})$= ~30	Shan and Tong (2013)
Iron–zirconium binaryoxide Co-precipitation; 339 (S); 5.1(IEP)	PSO; FIM; 120.0 (q_m); 25(t_{eq})	PSO; FIM; 46.1 (q_m); 25 (t_{eq})	Membrane	[As]=5- 40; [Ads]=0.2; pH=7; $\eta(SiO_3^{2-})$ =~60 and $\eta(PO_4^{3-})$)= ~40 for As III; $\eta(SiO_3^{2-})$ and $\eta(PO_4^{3-})$==~20 for As(V)	Ren et al. (2011)
Fe(III)–Al(III) mixed oxide Hydrothermal chemical precipitation; 15-22 (PS); 5.90 (pH_{PZC})	Endothermic; PSO; LIM; 58.30±3.15 (q_m); 1.5 (t_{eq})		NaOH(1-2 M); 50 (γ)	[As]=10–250; [Ads]=2.0; pH =7; T=30	Basu and Ghosh (2011)
$MnFe_2O_4$ and $CoFe_2O_4$ 30–50 (PS); 138 (S); 7.5 (pH_{PZC}); 32.02 (Ms) for $MnFe_2O_4$; 10–30(PS); 101 (S) 7.0 (pH_{PZC}) 46.99 (Ms) for $CoFe_2O_4$	PSO; LIM and FIM • For $MnFe_2O_4$ 93.8 (q_m) • For $CoFe_2O_4$ 100.3 (q_m) for	PSO; LIM and FIM • For $CoFe_2O_4$ 100.3 (q_m) for For $MnFe_2O_4$ 90.4 (q_m) • For $CoFe_2O_4$ 100.3 (q_m) for For $CoFe_2O_4$ 73.8 (q_m)	Magnetic; NaOH (0.1 and 1M) for For $MnFe_2O_4$; 87 for AsIII and 99 for AsV (γ)	[As]=0.5–50; [Ads]=0.2; pH= 7 for As(III) and 3 for As(V)	Zhang et al. (2010)
Iron(III)-Zirconium(IV) Binary Mixed Oxide 16-21 (PS); 6.8±0.2(pH_{PZC})	Endothermic; PSO; LIM and R-PI; 65.5±1.0 (q_m); 2(t_{eq})		NaOH or KOH (2.0 M); 80 (γ)	[As]=5-350; [Ads]=2; pH =7; T=30	Gupta et al. (2008)

PS (Average size of nanoparticles in nm); S (Surface area of nanoparticles in $m^2\ g^{-1}$); D (Average pore size of adsorbent in nm); dL (Lamellar thickness in nm); dM (Membrane thickness in μm); ρA (Mass surface density in mg cm^{-2}); Vp (Pore volume of adsorbent in cm^3g^{-1}); Ms (Saturation magnetization of adsorbent in emu g^{-1}); pH_{PZC} (Point Zero Charge of adsorbent); IEP (Isoelectric point); As(III), As(V) (Contaminant arsenic species); [As(III)] and [As(V)] (Initial arsenic concentration in mg L^{-1}); [Ads] (Adsorbent dose in gL^{-1}); T (Temperature °C); t_{eq} (Equilibrium time in Hour (h); η (Efficiency in %); Δη (Reduction of removal efficiency in %); q_m (Maximum adsorption capacity in mg g^{-1}); γ (Desorption efficiency in %); R (Arsenic recovery ratio in %); RC (Number of regeneration cycles); η_R (Residual efficiency after regeneration in %); PFO (Pseudo-First-order); PSO (Pseudo-Second-order); SO (Second-order); LIM (Langmuir isotherm model); FIM (Freundlich isotherm model); RPI (Redlich-Peterson isotherm model); * q_m values were represented in $\mu g.g^{-1}$.

within an initial 120 min, and the equilibrium was reached after 10 h (Table 1). Further, in another study, Bangari et al. (2020) observed that four folds increased the adsorption capacity of Fe_3O_4-functionalized boron nitride nanosheets (BNNS-Fe_3O_4 nanocomposite) compared with bare BNNSs for arsenic solution having initial concentration range between 6 and 70 ppm. The Langmuir isotherm model governed the adsorption process with the maximum adsorption capacity of 30.3 mg g^{-1} for As(III) at pH 8, while the adsorption kinetics followed the pseudo-second-order model. A decrease in ΔG° value from −15.35 to −16.92 (kJ mol^{-1}) at 298–318K suggested the favorability of the BNNS-Fe_3O_4 nanocomposite-mediated arsenic adsorption process at a higher temperature. Similarly, 160.65 mgg^{-1} of As(III) and 104.13 mgg^{-1} of As(V) were removed within 30 min by 1-butyl-3-methylimidazolium hexafluorophosphate ([BMIM][PF6])-(ionic liquid)-modified magnetic graphene oxide (MGO-IL) (Zhang et al., 2019). The adsorption process was endothermic and followed pseudo-second-order reaction kinetics. Adsorption of As(III) obeyed the Langmuir isotherm model, whereas favorability of the Freundlich model was observed in the case of As(V). The adsorption process was carried out in a wide pH range (2–12), where higher values of adsorption of As(V) at lower pH (< 4) were observed due to the electrostatic interaction of negatively charged As(V) ionic species and positively charged MGO-IL. In addition, electrostatic interaction was also reported between the imidazolium ring of the ionic liquid (IL) and As(V) anion. While adsorption of As(III) at higher pH (9) was attributed to the combined effect of electrostatic attraction, surface complexation, and formation of hydrogen bonds (Figure 2A). The removal efficiencies (%) of various studies conducted by multiple researchers are illustrated in Figure 3.

Furthermore, Tripathy et al. (2020) fabricated l-cysteine functionalized mesoporous Magnetite (Fe_3O_4@Cy) nanosphere using a surfactant-assisted solvothermal method with enhanced stability and adsorption efficiency. The adsorption process was reported to be spontaneous, endothermic, followed by pseudo-second-order reaction kinetics, and fitted well in the Langmuir isotherm model. The maximum adsorption capacities of Fe_3O_4@Cy nanoparticles were recorded as 20.0 and 34.0 mgg^{-1} for As(III) and As(V) ions, respectively. Rowley et al. (2019) investigated the adsorption capacity of 3-aminopro- pyltriethoxysilane (APTES)-Fe_3O_4 nanoparticles modified polyethersulfone (PES) nanocomposite membranes for As(V) removal from water. The adsorption capacity of the PES-A-Fe_3O_4) for As(V) gradually increased with an increasing percentage of APTES-Fe_3O_4 nanoparticles in PES membranes, and the maximum adsorption capacity (14.6 mg g^{-1}) was observed at 3% APTES-Fe_3O_4. Adsorption equilibrium was observed around 270 min. The

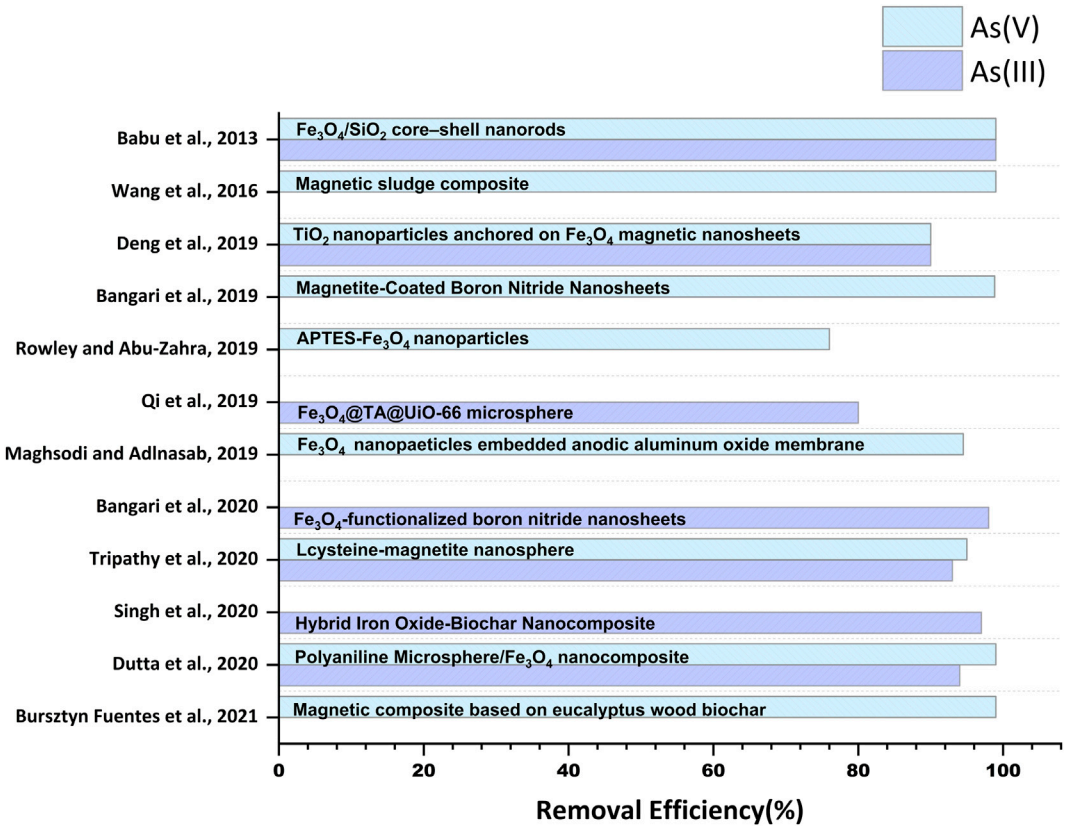

FIGURE 3
Arsenic removal *via* magnetite-based nanomaterials.

adsorption process followed the Freundlich isotherm, indicating the heterogeneous adsorption of As(V) onto the surface and dispersed APTES-Fe_3O_4 nanoparticles in the polymeric system. Pholosi et al. (2019) compared the As(III) adsorption by magnetite immobilized pine cone (MNP-PCP) with unmodified pine cone (PCP). They reported an increase in adsorption capacity from 14.83 mg g^{-1} (in PCP) to 18.02 mg g^{-1} (in MNP-PCP) at 299 K for As(III). Fe_3O_4 nanoparticles embedded on anodic aluminum oxide membrane (Fe_3O_4@ AAO) removed 83.3 mg g^{-1} of As(V) at pH 6 (Maghsodi et al., 2019). The adsorption process attained the equilibrium in 40 min at 25°C and fitted well with the Langmuir isotherm model. Moreover, the adsorption process was endothermic (ΔH° = 14.5 kJ mol^{-1}) and followed the linear pseudo-first-order. The negative value of Gibbs free energy change (ΔG° = −6.8214 kJ mol^{-1} at 298K) indicated the feasibility and spontaneous nature of As (V) adsorption Fe_3O_4@AAO membrane, which further increased with an increase in temperature. Additionally, the process could predict a suitable binding tendency between As(V) and Fe_3O_4@AAO membrane based on a change in entropy (ΔS° = 71.653J mol^{-1} K^{-1}). The same study reported the removal of 84.2%–94.5% arsenic from real water samples at pH 6 in 40 min (Figure 3). Detailed information regarding process parameters, kinetics, and adsorbents characteristics of the referred studies was tabulated in Table 1 and Table 2. However, most of the work was carried out under controlled laboratory conditions by using arsenic as a single source of contamination at fixed temperatures and pH. Data regarding multi-mixtures of contaminants in combination with arsenic are missing and need to be further explored under pilot-scale and environmental conditions.

3.1.2 Bimetallic iron oxide nanomaterials

Bimetallic nanomaterials exhibit novel molecular architecture and possess synergistic chemical and physical characteristics of constituent metals (Scaria et al., 2020). Improved reactivity, thermal stability, unique texture, magnetic properties, and tunable surface properties of bimetal oxides have drawn much interest from various researchers to evaluate the efficiency of this class of materials in catalytic removal of heavy metals and various oxyanions from contaminated water (Liu et al., 2014). Moreover, bimetallic nanomaterials or nanoalloys are inexpensive, readily available, and environmentally benign, making them preferable for designing affordable water treatment strategies (Zhang et al., 2013; Liu et al., 2014; Siddiqui et al., 2019; Sha et al., 2020). The structure of bimetallic (A_mB_n) NPs mainly depends on the nature of the constituent elements, synthesis pathways, A and B, their relative bond strengths, surface energies, relative atomic sizes, charge transfer, specific electronic/magnetic effects, and electronic perturbations in metal adatoms (Ferrando et al., 2008; Liu et al., 2014; Gilroy et al., 2016; Scaria et al., 2020).

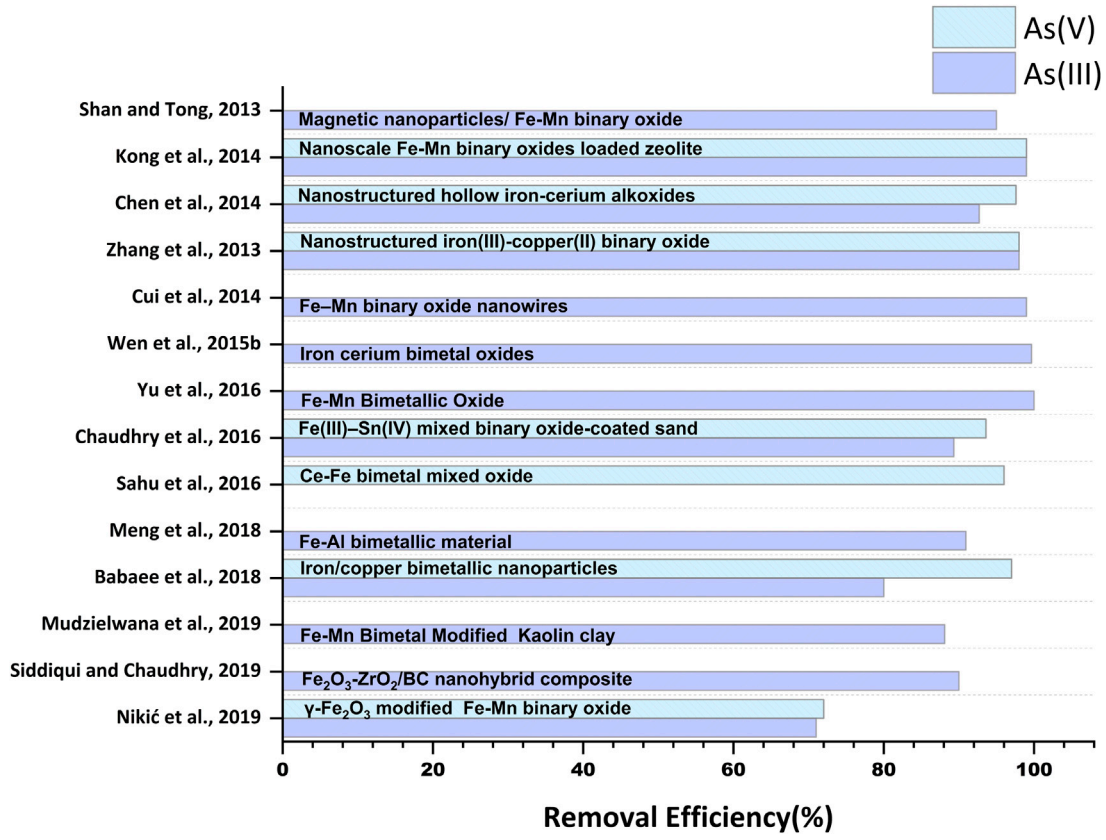

FIGURE 4
Arsenic removal *via* bimetallic iron oxide nanomaterials.

Wen et al. (2019) synthesized nanosized magnetic mesoporous Fe-Ce bimetal oxides (Nanosized-MMIC) to study the adsorption behavior for As(V). They reported that the adsorption of As(V) onto the nanosized-MMIC was attributed to the effective electrostatic interaction and formation of inner-sphere complexes between the adsorbent-adsorbate interface (Figure 2B). Nitrogen adsorption-desorption isotherm suggested the generation of ordered mesoporous metal oxide with 143.61 m^2g^{-1} surface area and 0.564 cm^3g^{-1} pore volume. The batch mode adsorption followed pseudo-second-order reaction kinetics, with the maximum adsorption capacity for As(V) being 111.17 mgg^{-1} at room temperature at pH 3. Another study reported by Wen et al. (2020) performed better adsorption of As(III) and As(V) on the magnetic ordered mesoporous Fe/Ce bimetal oxides (OMICs) compared to individual adsorption capacities of constituent pure mesoporous iron oxides and mesoporous cerium oxides. The adsorption process followed pseudo-second-order kinetics with maximum adsorption capacities of As(III) and As(V) for optimized adsorbent (calcined at 350°C for 3 h) were reported as 281.34 and 216.72 mg g^{-1}, respectively (Table 2). Chen et al. (2013b) reported that the maximum adsorption capacities of Ce-Fe oxide decorated multiwalled carbon nanotubes (CF-CNTs) for As(V) and As(III) were 30.96 and 28.74 mg g^{-1}, respectively. Partial oxidation of As(III) to As(V) before the adsorption has been reported. Further, As(V) adsorption onto CF-CNTs was attributed to the combined effect of adsorbate-adsorbent electrostatic interaction, surface complexation, and formation of both monodentate and bidentate complex on the adsorbent (CF-CNTs) surface.

Fe–Mn binary oxide could effectively oxidize As(III) to arsenate As(V) and remove both As(V) and As(III) from water (Zhang et al., 2014). X-ray absorption near-edge structure results indicated the existence of Mn atoms in a mixed-valence state of +3 and +4. MnO x (1.5 < x < 2) content was inferred to be responsible for the oxidation of As(III) to As(V) *via* two-step reduction of Mn(IV) to Mn(III) and subsequent Mn(III) to Mn(II) while adsorption of As(V) was attributed to FeOOH content in Fe-Mn binary oxides. However, no significant contribution of pure FeOOH was reported in the oxidation of As (III) in the presence of air. The study further confirmed the formation of the inner-sphere bidentate binuclear corner-sharing complex with As-M (M = Fe or Mn) interatomic distance of 3.22–3.24 Å in adsorbate-adsorbent surfaces. Mag-Fe-Mn particles (0.1 gL^{-1}) having maghemite core surrounded by amorphous Fe-Mn binary oxide coating lowered the concentration of As (III) from 200 μgL^{-1} to below 10 μgL^{-1} at pH 7 within 20 min with adsorption capacity 47.76 mgg^{-1} (Shan and Tong, 2013) (Figure 4). Complete oxidation of As (III) into As(V) was reported in the pH range 4–8. Heterogeneous adsorption of As (III) followed the pseudo-second-order kinetic model and fitted well in the Freundlich isotherm model and the two-site Langmuir model. Reduced graphene oxide (RGO) supported starch stabilized Fe-Mn binary oxide (Starch-FeMnOx) showed adsorption capacities of 78.74 mg g^{-1} and

55.56 mg g^{-1} for As(III) and As(V), respectively (Lou et al., 2017). Starch-FeMnOx/RGO exhibited 1.99 and 2.39 times more adsorption capacities for As(III) and As(V) than bare FeMnOx.

Another study (Cui et al., 2014) also reported complete oxidation of As(III) and lowering of 200 μg L^{-1} As(III) to below 10 μg L^{-1} in 75 min by magnetic porous Fe–Mn binary oxide nanowires (0.05 g L^{-1}) within the pH range 3–9. The adsorption capacity of Fe–Mn binary oxide nanowires was highest (171 mg g^{-1}) for the smallest Fe/Mn molar ratio 1:3 due to the enhanced peroxidation of As(III) in comparison to that in other Fe/Mn molar ratios (1:1 and 1:2). The Freundlich isotherm model and pseudo-second-order sorption kinetics are being used to explain the adsorption mechanism (Cui et al., 2014). Fe–Mn binary oxide encapsulated within a polystyrene anion exchanger D201 (D201-Fe/Mn) exhibited a maximum adsorption capacity of 44.91 mgg^{-1} and 13.17 mgg^{-1} for As(III) and As(V), respectively (Li et al., 2012). D201-Fe/Mn mediated arsenic adsorption was less sensitive to reaction pH over a wide pH range of 4–10 than Fe(III) oxide-loaded D201.

Wen et al. (2015b)showed that pre-oxidation of As(III) followed by adsorption of As(V) by Fenton-like magnetic mesoporous iron cerium bimetal oxide (MMIC) removed arsenic from water. After 60 min, there was approximately total oxidation of 1000 ppb A(III), and after 180 min, there was the total elimination of arsenic. XPS data and analysis of reactive oxidizing species indicated that As(III) was oxidized by the surface-bound •OH radicals of MMIC assigned to Fe^{2+} and Ce^{3+}. Further, free •OH generated by iron ions released from MMIC into bulk solution also influenced the arsenic adsorption process (Wen et al., 2015b).

As per the literature discussed above, the bimetallic system works better in terms of arsenic removal as well as it takes less time to complete the reaction. However, bimetallic systems depend highly on reaction variables such as temperature, pH, absorbent, and adsorbate concentration.

4 Parameters influencing the adsorption performance

The reaction parameters crucially impact the efficiency of the arsenic adsorption process are initial arsenic concentration, adsorbent dose, contact time, temperature, pH, and competing anions in water. Herein, the effect of such factors on the removal of arsenic in iron oxide (magnetite) and bimetallic iron oxide nanomaterials mediated adsorption process will be discussed in light of recently published literature.

4.1 Initial arsenic concentration and adsorbent dosages

The adsorption efficiency for a particular adsorbate-adsorbent system was directly proportional to the adsorbent concentration, which may be due to the abundance of vacant binding sites, and the reaction reaches the adsorption equilibrium quickly (Bangari et al., 2019; Siddiqui and Chaudhry, 2019). Initially, arsenic adsorption increases rapidly and reaches the saturation plateau at equilibrium after the saturation of binding sites present on the adsorbent surface (Dutta et al., 2020). However, excessive adsorbent doses reduce the adsorption efficiency due to a large amount of unoccupied binding sites and less availability of surface area (Wang et al., 2020). Wang et al. (2016) examined the adsorption capacity of magnetic bio-sludge (MS) containing activated sludge and magnetite (Fe_3O_4) nanoparticles in different initial arsenate concentrations (10, 50, 100, and 500 μg L^{-1}). The adsorption process was performed using 0.7 gL^{-1} of adsorbent dose for 5 h at 25°C. Almost complete As removal was observed at 10 μgL^{-1} initial As(V) concentrations. Chaudhry et al. (2016) observed significant changes in the arsenic adsorption efficiency of binaryFe(III)–Sn(IV) mixed oxide-coated sand (ITOCS) at different initial As concentrations. They suggested decrement could be associated with the saturation of binding sites on ITOCS. Sahu et al. (2016) reported a significant increment in As(V) removal with the increase in initial arsenic concentration from 0 to 10 mgL^{-1} by Ce-Fe bimetal mixed oxide. However, this study reported no prominent increase in As(V) removal after 10 mgL^{-1} of initial arsenic concentration.

4.2 Contact time and temperature

Process efficiency is greatly influenced by adsorbate-adsorbent contact time as shorter adsorption equilibrium signifies higher removal of As in smaller time intervals. Similarly, the reaction temperature can affect the activation energy of the adsorbat-adsorbent system, thus altering the adsorption performance. In endothermic adsorption, the reaction rate and adsorption capacity increase with the temperature rise, while exothermic processes are favored at low temperatures (Zhang et al., 2019; Wang et al., 2020). Liu et al. (2015a) reported spontaneous, endothermic adsorption of both As(III) and As(V) on crystalline magnetite nanoparticles (MNPs). Rapid adsorption was observed in the initial 5 min with an adsorption rate of 7.7 mmol g^{-1} h^{-1} and 6.7 mmol g^{-1} h^{-1} for As(V) and As (III), respectively, at pH 5. Furthermore, a slight increase in the maximum adsorption capacity for As(V) from 0.20 mmol g^{-1} to 0.25 mmol g^{-1} at 283 and 328 K was reported, while for As (III), the maximum adsorption capacity increased from 0.21 mmol g^{-1} to 0.23 mmol g^{-1} at 283K and 313 K respectively. Similarly, (Lin et al., 2017) observed a gradual increase in Fe-Mn modified biochar composite adsorption capacity from 8.09 to 8.45 mg g^{-1} for 288–308K. Also, another study conducted by Bangari et al. (2019) reported that adsorption of As onto Magnetite-coated boron nitride nanosheets (BNNS-Fe_3O_4) was endothermic between 10°C and 30°C whereas the process becomes exothermic after 30°C (30°C–40°C). This suggests that the initial increase in temperature provided enough energy for chemisorption, resulting in BNNS-Fe_3O_4 possessing a greater arsenic adsorption capability. However, a decrease in adsorption capacity was attributed to breaking adsorbate-adsorbent bonds with a further increase in temperature (beyond 30°C). A similar pattern of removal efficiency of Ce-Fe bimetal oxide for As(V) has been reported (Sahu et al., 2016).

4.3 Solution pH and coexisting anions

Iron oxide contains surface hydroxyl groups that get protonated or deprotonated with the pH of the solution (Deng et al., 2019).

Cheng et al. (2015) observed the point zero charge of nanosized magnetic iron oxide calcined at 250°C (FeMag-250) at about pH 7.5 and reported the maximum adsorption capacity (~50 mg g^{-1}) of FeMag-250 for As(III) at pH 7. The study suggested that the abundance of unaltered hydroxyl groups present on the adsorbent surface at pH 7 facilitates the adsorption of H_3AsO_3, while the scarcity of unaltered hydroxyl groups with further protonation at lower pH might reduce the adsorption capacity (~32 mg g^{-1}) of FeMag-250 for As(III) at pH 3. Further, a reduction in the adsorption capacity (~24.1) at higher pH could be attributed to the repulsion between arsenite anion and negatively charged adsorbent surface. Mag-Fe-Mn particles could remove 95% of As(III) within the pH range 4-8, while the removal efficiency of the adsorbent was reduced by 30% in the pH range 9–11 (Shan and Tong, 2013). Fe–Mn binary oxide nanowires removed 99% arsenic within the pH range three–nine and maintained residual arsenic below 10 μg L^{-1} (Cui et al., 2014). At a higher initial, As(III) concentration (5 mg L^{-1}), arsenic removal was found to be pH-dependent, and maximum arsenic removal efficiency was noted as 36.1% in acidic conditions, which further decreased with an increase in the pH of the solution. Dutta et al. (2020) reported the removal of ~94% As(III) and 98% As(V) from 1000 μg L^{-1} arsenic solution by polyaniline Microsphere/Fe_3O_4 nanocomposite (1 g L-1, pHpzc = 7.7) within optimum pH range of 3–7. However, adsorption of arsenic was inhibited above pH 9 due to the apparent electrostatic repulsion between negatively charged arsenic species and the adsorbent in excessive OH^- environment.

Coexistence of phosphate (PO_4^{3-}) sulfate (SO_4^{2-}), nitrate (NO_3^-), chloride (Cl^-), bicarbonate (HCO_3^-) and silicate (SiO_3^{2-}) ions resembling the similar surface charge architecture of anionic arsenic species can significantly impede the efficiency of arsenic removal processes (Deng et al., 2019; Nagarajan and Venkatanarasimhan, 2019). Presence of 01 mmol.L^{-1} SiO_3^{2-} and HPO_4^{2-} ions reduced the adsorption efficiency of FeMag-250 for As(III) from 93.9% to 78.5% and 60.9%, respectively (Cheng et al., 2015). The authors inferred that impedance in the adsorption occurred due to the similar structural property of $H_2PO^-_4$ and nearly identical pKa values of H_2SiO_3 as arsenite. However, no significant impact of SO_4^{2-}, NO_3^-, Cl^-, F^-, CO_3^{2-} on arsenic adsorption capacity of FeMag-250 was observed in the same study. Kumar et al. (2014) reported a negligible impact of SO_4^{2-}, NO_3^-, Cd^{2+} and Zn^{2+} on the arsenic adsorption efficiency of Graphene Oxide–$MnFe_2O_4$ magnetic nanohybrids (GONH). Coexistence of HCO_3^- (1 mM) reduced the adsorption efficiency of GONH from 96% to 89% in the case of As(III) and ~99.5% to 80% for As(V). Further, HPO_4^{2-} (1 mM) offered strong competition to arsenic species and suppressed the adsorption efficiency of GONH to 68% and 66% from 96% to 99.5% for As(III) and As(V), respectively, while SO_4^{2-}, NO_3^-, Cd^{2+} and Zn^{2+} imposed less effect on the arsenic adsorption performance.

Insignificant effect of coexisting Cl^-, NO_3^- and SO_4^{2-} was reported for As(III) adsorption by magnetic porous Fe–Mn binary oxide nanowires during the coexistence of PO_4^{3-} significantly decrease As(III) removal efficiency from 98.8% to 42.5% for 0–2 mM PO_4^{3-} concentration (Cui et al., 2014). Humic acid (HA) lowered the arsenic removal efficiency of Fe–Mn binary oxide nanowires leading to increased residual arsenic in the solution. It was reported that the residual arsenic concentration was below 10 μg L^{-1} for HA concentration <2 mg TOC L^{-1}, while a gradual increase of residual arsenic was observed for HA concentrations more than 2 mg TOC L^{-1}. However, the authors suggested that the residual arsenic concentration could be maintained below 10 μg L^{-1} by increasing the adsorbent dose. Lou et al. (2017) observed mild inhibition in the adsorption efficiency of Starch-FeMnOx/RGO composite-mediated arsenic adsorption for the coexistence of SO_4^{2-} (10 mM), while the coexistence of PO_4^{3-} declined the adsorption efficiency to 18.4% and 2.5% for As(III) and As(V), respectively. Furthermore, the study reported a decrease in the removal efficiency of As(III) and As(V) to 83.5% and 45.0% in the presence of 10 mM HCO_3^-.

5 Separation and regeneration of spent adsorbents

Separation of the arsenic-laden adsorbents from water is inevitable for the practical applicability of the adsorbent (Yavuz et al., 2006; Zhao et al., 2018) as it is important to avoid the generation of secondary pollutantsoriginating from the exhausted adsorbents (Hao et al., 2018). Several separation methods, such as centrifugation, filtration, gravitational sedimentation, and magnetic separation, have been considered to isolate the spent adsorbents from water (Lata and Samadder, 2016). The selection of the suitable desorbing agent depends upon the adsorbate-adsorbent interaction mechanism and the nature of the adsorbents. It has already been stated that the adsorption capacity of iron oxide-based adsorbent strongly depends upon their point of zero charges (PZC) values and the pH of the treatment system. Thus, alkaline solutions are often used for the desorption of anionic pollutants, while acidic solutions remove cationic contaminants from adsorbent surfaces (Wang et al., 2020). Numerous studies (Figure 5) have reported using NaOH, HCl, NaCl, and NaOCl to regenerate iron nanomaterial-based adsorbents (Rajesh Kumar et al., 2016; Yu et al., 2018; Nikić et al., 2021). However, NaOH was commonly used for arsenic desorption from iron nanomaterial-based adsorbents. Spherical polystyrene-supported nano-Fe_3O_4 beads (PS-Fe_3O_4) of 350–400 nm in diameter were successfully separated from water by a low-field separation method under a magnetic field of intensity <0.035 T in 15 min (Jiang et al., 2012). Desorption of arsenate from magnetically separated exhausted adsorbent was carried out by dispersing the spent adsorbent in 0.10 mol L^{-1} NaOH solution for 2 h, followed by centrifugation and cleaning with deionized water. The adsorption efficiency of PS-Fe_3O_4 for As(V) was 93.8% after the sixth adsorption-regeneration cycle, while the adsorption capacities decreased from 10.6 to 9.5 mgg^{-1}. Powell et al. (2020) removed more than 94% of arsenic-laden iron oxide nanoparticles (As-Fe_3O_4) using a magnetic nanoparticle recovery device (MagNERD) after arsenic treatment. Zhang et al. (2019) reported a promising saturation magnetization value of 27.79 emu g-1 of ionic liquid-modified magnetic graphene oxide (MGO-IL). The authors reported rapid magnetic isolation of MGO-IL from aqueous solution with a negligible decrease in adsorption capacity 8.06%

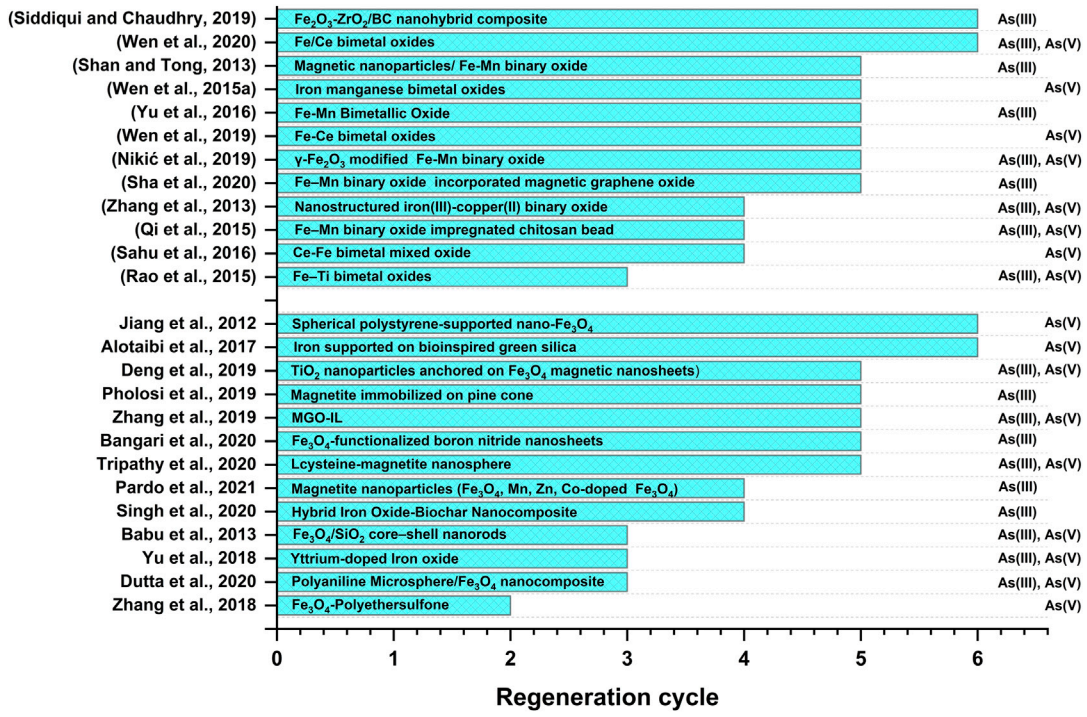

FIGURE 5
Reuse cycles of adsorbents.

for As(III) and 14.14% for As(V), respectively, after the fifth adsorption-regeneration cycle. Kumar et al. (2014) separated a superparamagnetic GO-$MnFe_2O_4$ hybrid (GONH) from an aqueous solution using an external magnetic field. Efficient recovery of 99% As(V) and 93% As(III) from spent GONH in 1M NaOH solution has been reported in the literature. Similarly, significant retention (95%) of the removal efficiency was reported in nanosized iron oxide (FeMag) for As(III) after five adsorption-regeneration cycles by treating with 1 $molL^{-1}$ NaOH solution for 6 h (Cheng et al., 2015). Desorption of anionic arsenic species from the FeMag surface was attributed to the hydroxyl ion exchange and electrostatic repulsion on the adsorbent-adsorbate interface.

Dutta et al. (2020) reported ~83% retention of initial adsorption efficiency for As(III) in polyaniline Microsphere/Fe_3O_4 nanocomposite after the third regeneration cycle at 300 ± 3 K. Similarly, 86% and 90% removal efficiency for As(III) were reported for iron oxide-rice husk hybrid biochar nanocomposite and iron oxide-wheat husk hybrid biochar nanocomposite after the fourth regeneration cycle using NaOH (0.1 N) and NaCl (0.1 N) (Singh et al., 2020). Similarly, Sha et al. (2020) reported only a 5.1% loss of adsorption efficiency by magnetic graphene oxide (MRGO)– Fe–Mn binary oxide (FMBO) after five recycling cycles.

It was reported that higher desorption (97.58%) for As(V) could achieve in Ce- Fe bimetal oxide by increasing the concentration of NaOH (0.5M) solution (Sahu et al., 2016). A ternary solution composed of NaOH, NaCl, and NaClO could efficiently regenerate D201-Fe/Mn (Li et al., 2012). The authors reported that NaOH and NaCl could desorb arsenic from the exhausted adsorbent while NaClO oxidized Mn(II) to Mn(IV). Similarly, Mag-Fe-Mn particles obtained *via* magnetic separation were regenerated using a ternary solution consisting of NaOH, NaCl, and NaClO (Shan and Tong, 2013). Mag-Fe-Mn particles exhibited 87% desorption efficiency and 98% of adsorption efficiency for As(III) throughout five adsorption-regeneration cycles.

6 Insight on toxicity and biocompatibility

Possible migration of nano solids (pristine and pollutant-laden) during water decontamination processes could impose potential risk upon its end users and various organisms in natural systems (Morillo et al., 2016; Simeonidis et al., 2016). Hence, a closer assessment of the toxicity of nanomaterials is a dire necessity before the mass application of nanomaterial-mediated water purification systems. Accumulated research suggested that iron oxide nanoparticle-mediated toxicity greatly depends on the pathways of the entry of nanoparticles into organisms (Frtús et al., 2020; Chrishtop et al., 2021). The toxicity of iron oxide nanoparticles could be assigned to the production of reactive oxygen species and subsequent oxidative stress in nanoparticle-mediated metabolic processes (Wu et al., 2014; Frtús et al., 2020). Oral

administration of iron oxide nanoparticles significantly increases the nanoparticle load on the liver and kidneys, while iron oxide nanoparticles entered through the sensory route could cross the blood-brain barrier in animals and cause neurotoxicity (Chrishtop et al., 2020). Iron oxide nanoparticles at high concentrations could impose severerisk due to higher accumulation in various organs and difficulties in their efficient excretion from the organism's body (Mou et al., 2015; Chrishtop et al., 2020). Despite some toxicological constraints, various studies supported the biocompatibility of iron oxide nanoparticles. Mahanty et al. (2019) reported insignificant changes in resazurin reduction by suspended *E. coli* culture in the presence of uncoated, citric acid coated and polyethylene glycol coated Fe_3O_4 nanoparticles in comparison to nanoparticle-free control, while the toxic effect of methacrylic acid coated Fe_3O_4 nanoparticles was observed during the study. The authors reported moderate toxicity in the soil microcosm of all the Fe3O4 nanoparticle variants. Further, Fe_3O_4 nanoparticle-induced toxicity was reduced with soil ageing, which could be attributed to the metal solubilisation, changes in their availability or biogeochemical interactions that occurred during the aging process.

Iannone et al. (2016) reported insignificant changes in germination rate, chlorophyll content, electrolyte release, cell death percentage, and growth in wheat (*Triticum aestivum L.)* plants for 5–20 mgL^{-1} of Fe_3O_4 nanoparticle. Accumulation of Fe_3O_4 nanoparticles in the roots of treated plants was observed. However, no translocation of nanoparticles into leaves was reported. Their study found no significant changes in lipid peroxidation and H_2O_2 accumulation in Fe_3O_4 nanoparticles treated plants with respect to their control counterparts.

Ledda et al. (2020) designed sub-5 nm silica-coated superparamagnetic iron oxide (sub-5 SIO-Fl) nanoparticles for oncology-related theranostics applications. This study observed the quick absorption of nanoparticles within 24 h of treatment; however, a gradual decrement in uptake was observed after 48 h. Additionally, no sign of kidney, spleen, stomach, or liver necrosis was reported until 7 weeks afterthe nanoparticles injection. Nguyen et al. (2020) observed a significant decrement in copper toxicity by using Fe-Cu bimetallic oxide nanoparticles (500 μg mL^{-1}) for the treatment of rat kidney proximal tubule epithelial cells (NRK-52E). About 94% survival rate was observed in Fe-Cu bimetallic oxide nanoparticles treated NRK-52E cell line while the control (CuO) shows great decrement in survivability (8%). Whereas approximately 100% survival rate was observed for Fe_3O_4 nanoparticles on the same cell lines using similar concentrations. Fe-Cu nanocomposite treatment showed faster healing of diabetic wounds in methicillin-resistant *S. aureus* (MRSA) infected Wistar albino rats than iodine-treated and untreated groups over 21 days (Das et al., 2019). Further, the same literature reported 0.29% and 0.32% hemolysis in nanocomposite-treated human erythrocytes for nanocomposite powder and nanocomposite-impregnated cotton, respectively, is relatively lower than the permissible limit (5%) for blood containing biomaterial.

The accumulated data suggested the biocompatibility and low toxicity of iron oxide nanoparticles in target organisms. However, more data is required to evaluate the toxicity and biocompatibility of bimetallic iron oxide nanoparticles. It has been observed that iron oxide nanoparticle-mediated toxicity could be assigned to its physical and chemical characteristics. Indeed, iron oxide nanoparticle-induced toxicity is target specific and closely related to the properties of nanoparticle coating materials. Possible causes of iron oxide toxicity could be summarized as nanoparticle-induced oxidative stress, ROS production, autophagy, apoptosis, cell migration, inhibitory effect on osteoclastogenesis, inflammation and cell death, transient phenotypic changes of macrophages, cell cycle arrest, activation of dendritic cells in different cell models (Frtús et al., 2020). Research on the molecular mechanisms of nanoparticle-cell interaction is necessary to evaluate nanoparticle-induced toxicity and its biocompatibility. Impact assessment of external stimuli, such as light water chemistry on the surface-bound ligands of nanoparticles, could be helpful in understanding the dynamics of nanoparticle release in nanomaterial-mediated water decontamination systems (Frtús et al., 2020; Nagar and Pradeep, 2020).

7 Conclusion

Arsenic adsorption was found to be predominated by surface complexation (electrostatic interaction, chemisorption, hydroxyl radical influence adsorption process) and ligand exchange onto the nanomaterials surface, while oxidation of As(III) to As(V) before adsorption has been reported in case of some manganese-containing bimetallic iron oxide nanomaterials. Bimetallic systems are more effective and require less time for reaction completion. The Fe-Mn bimetallic oxide nanomaterials showed promising trends in arsenic removal due to the synergistic oxidation and adsorption of highly toxic As(III) from water. The aqueous medium's pH significantly impacts the As adsorption process, which can be effectively described by the Langmuir and Freundlich isotherm models. The remarkable magnetic properties of iron-based nanomaterials facilitate their easy magnetic separation from treated water which makes magnetic nanomaterials advantageous over non-magnetic adsorbents. Results revealed that magnetite and bimetallic-based adsorption could be safely used up to four to five and three to four regeneration cycles. However, the presented document revealed that majorly studies were carried out under controlled laboratory conditions, but research is needed to verify them under natural environmental conditions. Furthermore, this review article will help scientists and researchers decide which combinations of iron nanomaterials were used for arsenic removal from water.

8 Future research directions and key challenges

Despite notable achievements in arsenic removal by nanomaterials, specific challenges still need to be addressed before the successful implementation of nanomaterial-mediated

arsenic removal processes on a large scale. The design and implementation of magnetite and bimetallic iron oxide nanomaterials with suitable adsorption characteristics and the applications in As elimination from water should be addressed coherently to optimize. Despite the fact that the applications have been extensively described in the literature, several study scopes (open research topics) remain to be explored.

1. In most of the investigations, the adsorbent was constructed by incorporating nanophase into a suitable substrate or host to enhance the stability of adsorbents and reduce the migration of nanomaterials into product water. However, the biocompatibility and toxicity of nanoparticle coating materials and hosts/substrates need to be evaluated to eliminate the secondary risk associated with magnetite and bimetallic iron oxide nanomaterials.
2. There is a need for further improvements in the adsorption capability of magnetite and bimetallic iron oxide nanomaterial, whether from adsorption rate or capacity. This can be achieved by optimizing particle/pore shapes and sizes, imparting suitable functional groups onto the surface depending on the As properties, or by modulating the synthesis conditions to maximize active adsorption sites. Most of the studies were carried out under controlled laboratory conditions, and minimal studies have been reported using real water matrices, thus making the practical application of adsorbents difficult. Hence, more research is needed to demystify the uncertainties in the effectivity and hydrodynamic stability of magnetite and bimetallic iron oxide nanomaterials in complex real water matrices under regulated conditions (such as low initial concentration of As, neutral pH, atmospheric temperature, and the presence of other pollutants); and ranked them based on their importance.
3. Regeneration and reusability of spent adsorbents (of magnetite and bimetallic iron oxide nanomaterial) determine the cost efficiency of water decontamination processes. Although most of the adsorbents cited here showed promising adsorption capacity for arsenic removal after four to five adsorption-regeneration cycles (Figure 5), improvements are still required to enhance the affordability and sustainability of the adsorbents.
4. Leaching tests are also needed to successfully implement iron-based adsorption processes under natural environmental conditions.
5. Life cycle assessment of nanomaterials and long-term monitoring of arsenic-laden adsorbents could be helpful to evaluate the environmental sustainability of nanomaterials enabled As adsorption processes.
6. There is a need to understand the compatibility of iron-based nanomaterials as per the characteristics of water where arsenic is present.

Author contributions

HB: Conceptualization, Writing - original draft, Formal analysis; NT: Visualization, Writing - review & editing; SG: Writing - review & editing; MC: Conceptualization, Writing - review & editing, Visualization, Supervision. TM: Writing - review & editing.

Conflict of interest

The authors declare that the research was conducted in the absence of any commercial or financial relationships that could be construed as a potential conflict of interest.

Publisher's note

All claims expressed in this article are solely those of the authors and do not necessarily represent those of their affiliated organizations, or those of the publisher, the editors and the reviewers. Any product that may be evaluated in this article, or claim that may be made by its manufacturer, is not guaranteed or endorsed by the publisher.

Supplementary material

The Supplementary Material for this article can be found online at: https://www.frontiersin.org/articles/10.3389/fenvs.2023.1104320/full#supplementary-material

SUPPLEMENTARY FIGURE S1
Graphical representation of arsenic removal from water via Iron nanomaterial based adsorbents.

References

Alotaibi, K. M., Shiels, L., Lacaze, L., Peshkur, T. A., Anderson, P., Machala, L., et al. (2017). Iron supported on bioinspired green silica for water remediation. *Chem. Sci.* 8, 567–576. doi:10.1039/C6SC02937J

Arslan, H., Gonca, S., Isik, Z., Özdemir, S., Yalvac, M., Dizge, N., et al. (2022). Iron oxide nanoparticles synthesis from vermicomposting leachate and its antioxidant activities. *Front. Mat.* 9, 912066. doi:10.3389/fmats.2022.912066

Babaee, Y., Mulligan, C. N., and Rahaman, M. S. (2018). Removal of arsenic (III) and arsenic (V) from aqueous solutions through adsorption by Fe/Cu nanoparticles. *J. Chem. Technol. Biotechnol.* 93, 63–71. doi:10.1002/jctb.5320

Babu, C. M., Palanisamy, B., Sundaravel, B., Palanichamy, M., and Murugesan, V. (2013). A novel magnetic Fe_3O_4/SiO_2 core–shell nanorods for the removal of arsenic. *J. Nanosci. Nanotechnol.* 13, 2517–2527. doi:10.1166/jnn.2013.7376

Bangari, R. S., Singh, A. K., Namsani, S., Singh, J. K., and Sinha, N. (2019). Magnetite-coated boron nitride nanosheets for the removal of arsenic(V) from water. *ACS Appl. Mat. Interfaces* 11, 19017–19028. doi:10.1021/acsami.8b22401

Bangari, R. S., Yadav, V. K., Singh, J. K., and Sinha, N. (2020). Fe_3O_4-Functionalized boron nitride nanosheets as novel adsorbents for removal of arsenic(III) from contaminated water. *ACS Omega* 5, 10301–10314. doi:10.1021/acsomega.9b04295

Basu, T., and Ghosh, U. C. (2011). Arsenic(III) removal performances in the absence/presence of groundwater occurring ions of agglomerated Fe(III)-Al(III) mixed oxide nanoparticles. *J. Ind. Eng. Chem.* 17, 834–844. doi:10.1016/j.jiec.2011.09.002

Bhardwaj, P., Kaur, N., Selvaraj, M., Ghramh, H. A., Al-Shehri, B. M., Singh, G., et al. (2022). Laccase-assisted degradation of emerging recalcitrant compounds-A review. *Bioresour. Technol.* 364, 128031. doi:10.1016/j.biortech.2022.128031

Bursztyn Fuentes, A. L., Barraqué, F., Mercader, R. C., Scian, A. N., and Montes, M. L. (2021). Efficient low-cost magnetic composite based on eucalyptus wood biochar for arsenic removal from groundwater. *Groundw. Sustain. Dev.* 14, 100585. doi:10.1016/j.gsd.2021.100585

Chatterjee, S., Mahanty, S., Das, P., Chaudhuri, P., and Das, S. (2020). Biofabrication of iron oxide nanoparticles using manglicolous fungus Aspergillus Niger BSC-1 and

removal of Cr (VI) from aqueous solution. *Chem. Eng. J.* 385, 123790. doi:10.1016/j.cej.2019.123790

Chaudhry, S. A., Ahmed, M., Siddiqui, S. I., and Ahmed, S. (2016). Fe(III)–Sn(IV) mixed binary oxide-coated sand preparation and its use for the removal of As(III) and As(V) from water: Application of isotherm, kinetic and thermodynamics. *J. Mol. Liq.* 224, 431–441. doi:10.1016/j.molliq.2016.08.116

Chen, B., Zhu, Z., Guo, Y., Qiu, Y., and Zhao, J. (2013a). Facile synthesis of mesoporous Ce-Fe bimetal oxide and its enhanced adsorption of arsenate from aqueous solutions. *J. Colloid Interface Sci.* 398, 142–151. doi:10.1016/j.jcis.2013.02.004

Chen, B., Zhu, Z., Liu, S., Hong, J., Ma, J., Qiu, Y., et al. (2014). Facile hydrothermal synthesis of nanostructured hollow iron-cerium alkoxides and their superior arsenic adsorption performance. *ACS Appl. Mat. Interfaces* 6, 14016–14025. doi:10.1021/am503343u

Chen, B., Zhu, Z., Ma, J., Qiu, Y., and Chen, J. (2013b). Surfactant assisted Ce-Fe mixed oxide decorated multiwalled carbon nanotubes and their arsenic adsorption performance. *J. Mat. Chem. A* 1, 11355–11367. doi:10.1039/c3ta11827d

Chen, W., Wu, J., Weng, X., Owens, G., and Chen, Z. (2022). One-step green synthesis of hybrid Fe-Mn nanoparticles: Methodology, characterization and mechanism. *J. Clean. Prod.* 363, 132406. doi:10.1016/j.jclepro.2022.132406

Cheng, W., Xu, J., Wang, Y., Wu, F., Xu, X., and Li, J. (2015). Dispersion-precipitation synthesis of nanosized magnetic iron oxide for efficient removal of arsenite in water. *J. Colloid Interface Sci.* 445, 93–101. doi:10.1016/j.jcis.2014.12.082

Chilvers, B. L., Morgan, K. J., and White, B. J. (2021). Sources and reporting of oil spills and impacts on wildlife 1970–2018. *Environ. Sci. Pollut. Res.* 28, 754–762. doi:10.1007/s11356-020-10538-0

Chrishtop, V. V., Mironov, V. A., Prilepskii, A. Y., Nikonorova, V. G., and Vinogradov, V. V. (2021). Organ-specific toxicity of magnetic iron oxide-based nanoparticles. *Nanotoxicology* 15, 167–204. doi:10.1080/17435390.2020.1842934

Cui, H. J., Cai, J. K., Zhao, H., Yuan, B., Ai, C. L., and Fu, M. L. (2014). Fabrication of magnetic porous Fe-Mn binary oxide nanowires with superior capability for removal of As(III) from water. *J. Hazard. Mat.* 279, 26–31. doi:10.1016/j.jhazmat.2014.06.054

Das, M., Goswami, U., Kandimalla, R., Kalita, S., Ghosh, S. S., and Chattopadhyay, A. (2019). Iron-copper bimetallic nanocomposite reinforced dressing materials for infection control and healing of diabetic wound. *ACS Appl. Bio Mat.* 2, 5434–5445. doi:10.1021/acsabm.9b00870

De, D., Mandal, S. M., Bhattacharya, J., Ram, S., and Roy, S. K. (2009). Iron oxide nanoparticle-assisted arsenic removal from aqueous system. *J. Environ. Sci. Heal. - Part A Toxic/Hazardous Subst. Environ. Eng.* 44, 155–162. doi:10.1080/10934520802539756

Deng, M., Wu, X., Zhu, A., Zhang, Q., and Liu, Q. (2019). Well-dispersed TiO_2 nanoparticles anchored on Fe_3O_4 magnetic nanosheets for efficient arsenic removal. *J. Environ. Manage.* 237, 63–74. doi:10.1016/j.jenvman.2019.02.037

Dutta, S., Manna, K., Srivastava, S. K., Gupta, A. K., and Yadav, M. K. (2020). Hollow polyaniline microsphere/Fe_3O_4 nanocomposite as an effective adsorbent for removal of arsenic from water. *Sci. Rep.* 10, 4982. doi:10.1038/s41598-020-61763-z

Ferguson, J. F., and Gavis, J. (1972). A review of the arsenic cycle in natural waters. *Water Res.* 6, 1259–1274. doi:10.1016/0043-1354(72)90052-8

Ferrando, R., Jellinek, J., and Johnston, R. L. (2008). Nanoalloys: From theory to applications of alloy clusters and nanoparticles. *Chem. Rev.* 108, 845–910. doi:10.1021/cr040090g

Frtús, A., Smolková, B., Uzhytchak, M., Lunova, M., Jirsa, M., Kubinová, Š., et al. (2020). Analyzing the mechanisms of iron oxide nanoparticles interactions with cells: A road from failure to success in clinical applications. *J. Control. Release* 328, 59–77. doi:10.1016/j.jconrel.2020.08.036

Gilroy, K. D., Ruditskiy, A., Peng, H. C., Qin, D., and Xia, Y. (2016). Bimetallic nanocrystals: Syntheses, properties, and applications. *Chem. Rev.* 116, 10414–10472. doi:10.1021/acs.chemrev.6b00211

Gupta, K., Biswas, K., and Ghosh, U. C. (2008). Nanostructure iron(III)-zirconium(IV) binary mixed oxide: Synthesis, characterization, and physicochemical aspects of arsenic(III) sorption from the aqueous solution. *Ind. Eng. Chem. Res.* 47, 9903–9912. doi:10.1021/ie8002107

Hao, L., Liu, M., Wang, N., and Li, G. (2018). A critical review on arsenic removal from water using iron-based adsorbents. *RSC Adv.* 8, 39545–39560. doi:10.1039/c8ra08512a

Huong, P. T. L., Huy, L. T., Lan, H., Thang, L. H., An, T. T., Van Quy, N., et al. (2018). Magnetic iron oxide-carbon nanocomposites: Impacts of carbon coating on the As(V) adsorption and inductive heating responses. *J. Alloys Compd.* 739, 139–148. doi:10.1016/j.jallcom.2017.12.178

Iannone, M. F., Groppa, M. D., de Sousa, M. E., Fernández van Raap, M. B., and Benavides, M. P. (2016). Impact of magnetite iron oxide nanoparticles on wheat (*Triticum aestivum L.*) development: Evaluation of oxidative damage. *Environ. Exp. Bot.* 131, 77–88. doi:10.1016/j.envexpbot.2016.07.004

Jaspal, D., and Malviya, A. (2020). Composites for wastewater purification: A review. *Chemosphere* 246, 125788. doi:10.1016/j.chemosphere.2019.125788

Jiang, W., Chen, X., Niu, Y., and Pan, B. (2012). Spherical polystyrene-supported nano-Fe_3O_4 of high capacity and low-field separation for arsenate removal from water. *J. Hazard. Mat.* 243, 319–325. doi:10.1016/j.jhazmat.2012.10.036

Kokate, M., Garadkar, K., and Gole, A. (2013). One pot synthesis of magnetite-silica nanocomposites: Applications as tags, entrapment matrix and in water purification. *J. Mat. Chem. A* 1, 2022–2029. doi:10.1039/c2ta00951j

Kong, S., Wang, Y., Hu, Q., and Olusegun, A. K. (2014). Magnetic nanoscale Fe-Mn binary oxides loaded zeolite for arsenic removal from synthetic groundwater. *Colloids Surfaces A Physicochem. Eng. Asp.* 457, 220–227. doi:10.1016/j.colsurfa.2014.05.066

Kumar, S., Nair, R. R., Pillai, P. B., Gupta, S. N., Iyengar, M. A. R., and Sood, A. K. (2014). Graphene oxide-$MnFe_2O_4$ magnetic nanohybrids for efficient removal of lead and arsenic from water. *ACS Appl. Mat. Interfaces* 6, 17426–17436. doi:10.1021/am504826q

Lafferty, B. J., Ginder-Vogel, M., and Sparks, D. L. (2010). Arsenite oxidation by a poorly crystalline manganese-oxide 1. stirred-flow experiments. *Environ. Sci. Technol.* 44, 8460–8466. doi:10.1021/es102013p

Lata, S., and Samadder, S. R. (2016). Removal of arsenic from water using nano adsorbents and challenges: A review. *J. Environ. Manage.* 166, 387–406. doi:10.1016/j.jenvman.2015.10.039

Ledda, M., Fioretti, D., Lolli, M. G., Papi, M., Di Gioia, C., Carletti, R., et al. (2020). Biocompatibility assessment of sub-5 nm silica-coated superparamagnetic iron oxide nanoparticles in human stem cells and in mice for potential application in nanomedicine. *Nanoscale* 12, 1759–1778. doi:10.1039/c9nr09683c

Li, X., He, K., Pan, B., Zhang, S., Lu, L., and Zhang, W. (2012). Efficient As(III) removal by macroporous anion exchanger-supported Fe-Mn binary oxide: Behavior and mechanism. *Chem. Eng. J.* 193, 131–138. doi:10.1016/j.cej.2012.04.036

Lin, L., Qiu, W., Wang, D., Huang, Q., Song, Z., and Chau, H. W. (2017). Arsenic removal in aqueous solution by a novel Fe-Mn modified biochar composite: Characterization and mechanism. *Ecotoxicol. Environ. Saf.* 144, 514–521. doi:10.1016/j.ecoenv.2017.06.063

Lin, L., Yang, H., and Xu, X. (2022). Effects of water pollution on human health and disease heterogeneity: A review. *Front. Environ. Sci.* 10, 880246. doi:10.3389/fenvs.2022.880246

Liu, B., Kim, K. H., Kumar, V., and Kim, S. (2020). A review of functional sorbents for adsorptive removal of arsenic ions in aqueous systems. *J. Hazard. Mat.* 388, 121815. doi:10.1016/j.jhazmat.2019.121815

Liu, C. H., Chuang, Y. H., Chen, T. Y., Tian, Y., Li, H., Wang, M. K., et al. (2015a). Mechanism of arsenic adsorption on magnetite nanoparticles from water: Thermodynamic and spectroscopic studies. *Environ. Sci. Technol.* 49, 7726–7734. doi:10.1021/acs.est.5b00381

Liu, S., Kang, S., Wang, G., Zhao, H., and Cai, W. (2015b). Micro/nanostructured porous Fe-Ni binary oxide and its enhanced arsenic adsorption performances. *J. Colloid Interface Sci.* 458, 94–102. doi:10.1016/j.jcis.2015.07.038

Liu, W. J., Qian, T. T., and Jiang, H. (2014). Bimetallic Fe nanoparticles: Recent advances in synthesis and application in catalytic elimination of environmental pollutants. *Chem. Eng. J.* 236, 448–463. doi:10.1016/j.cej.2013.10.062

Lou, Z., Cao, Z., Xu, J., Zhou, X., Zhu, J., Liu, X., et al. (2017). Enhanced removal of As(III)/(V) from water by simultaneously supported and stabilized Fe-Mn binary oxide nanohybrids. *Chem. Eng. J.* 322, 710–721. doi:10.1016/j.cej.2017.04.079

Maghsodi, A., and Adlnasab, L. (2019). *In-situ* chemical deposition as a new method for the preparation of Fe_3O_4 nanopaeticles embedded on anodic aluminum oxide membrane (Fe_3O_4@AAO): Characterization and application for arsenic removal using response surface methodology. *J. Environ. Chem. Eng.* 7, 103288. doi:10.1016/j.jece.2019.103288

Mahanty, B., Jesudas, S., and Padmaprabha, A. (2019). Toxicity of surface functionalized iron oxide nanoparticles toward pure suspension culture and soil microcosm. *Environ. Nanotechnol. Monit. Manag.* 12, 100235. doi:10.1016/j.enmm.2019.100235

Majumder, A., Ramrakhiani, L., Mukherjee, D., Mishra, U., Halder, A., Mandal, A. K., et al. (2019). Green synthesis of iron oxide nanoparticles for arsenic remediation in water and sludge utilization. *Clean Technol. Environ. Policy* 21, 795–813. doi:10.1007/s10098-019-01669-1

McDonald, K. J., Reynolds, B., and Reddy, K. J. (2015). Intrinsic properties of cupric oxide nanoparticles enable effective filtration of arsenic from water. *Sci. Rep.* 51 (5), 11110–10. doi:10.1038/srep11110

Mehta, D., Mazumdar, S., and Singh, S. K. (2015). Magnetic adsorbents for the treatment of water/wastewater-A review. *J. Water Process Eng.* 7, 244–265. doi:10.1016/j.jwpe.2015.07.001

Meng, C., Mao, Q., Luo, L., Zhang, J., Wei, J., Yang, Y., et al. (2018). Performance and mechanism of As(III) removal from water using Fe-Al bimetallic material. *Sep. Purif. Technol.* 191, 314–321. doi:10.1016/j.seppur.2017.09.051

Moosavi, S., Lai, C. W., Gan, S., Zamiri, G., Akbarzadeh Pivehzhani, O., and Johan, M. R. (2020). Application of efficient magnetic particles and activated carbon for dye removal from wastewater. *ACS Omega* 5, 20684–20697. doi:10.1021/acsomega.0c01905

Moreira, V. R., Lebron, Y. A. R., Santos, L. V. S., Coutinho de Paula, E., and Amaral, M. C. S. (2021). Arsenic contamination, effects and remediation techniques: A special look onto membrane separation processes. *Process Saf. Environ. Prot.* 148, 604–623. doi:10.1016/j.psep.2020.11.033

Morillo, D., Faccini, M., Amantia, D., Pérez, G., García, M. A., Valiente, M., et al. (2016). Superparamagnetic iron oxide nanoparticle-loaded polyacrylonitrile nanofibers with enhanced arsenate removal performance. *Environ. Sci. Nano* 3, 1165–1173. doi:10.1039/c6en00167j

Morillo, D., Pérez, G., and Valiente, M. (2015a). Efficient arsenic(V) and arsenic(III) removal from acidic solutions with Novel Forager Sponge-loaded superparamagnetic iron oxide nanoparticles. *J. Colloid Interface Sci.* 453, 132–141. doi:10.1016/j.jcis.2015.04.048

Morillo, D., Uheida, A., Pérez, G., Muhammed, M., and Valiente, M. (2015b). Arsenate removal with 3-mercaptopropanoic acid-coated superparamagnetic iron oxide nanoparticles. *J. Colloid Interface Sci.* 438, 227–234. doi:10.1016/j.jcis.2014.10.005

Mou, X., Ali, Z., Li, S., and He, N. (2015). Applications of magnetic nanoparticles in targeted drug delivery system. *J. Nanosci. Nanotechnol.* 15, 54–62. doi:10.1166/jnn.2015.9585

Mudzielwana, R., Gitari, W. M., and Ndungu, P. (2019). Removal of as(III) from synthetic groundwater using Fe-Mn bimetal modified kaolin clay: Adsorption kinetics, isotherm and thermodynamics studies. *Environ. Process.* 6, 1005–1018. doi:10.1007/s40710-019-00397-4

Nagar, A., and Pradeep, T. (2020). Clean water through nanotechnology: Needs, gaps, and fulfillment. *ACS Nano* 14, 6420–6435. doi:10.1021/acsnano.9b01730

Nagarajan, D., and Venkatanarasimhan, S. (2019). Magnetite microparticles decorated cellulose sponge as an efficacious filter for improved arsenic(V) removal. *J. Environ. Chem. Eng.* 7, 103386. doi:10.1016/j.jece.2019.103386

Nazari, A., Nakhaei, M., and Yari, A. R. (2020). Arsenic adsorption by TiO_2 nanoparticles under conditions similar to groundwater: Batch and column studies. *Int. J. Environ. Res.* 15, 79–91. doi:10.1007/s41742-020-00298-7

Nguyen, T. B., Dong, C. D., Huang, C. P., Chen, C. W., Hsieh, S. L., and Hsieh, S. (2020). Fe-Cu bimetallic catalyst for the degradation of hazardous organic chemicals exemplified by methylene blue in Fenton-like reaction. *J. Environ. Chem. Eng.* 8, 104139. doi:10.1016/j.jece.2020.104139

Nikić, J., Watson, M. A., Isakovski, M. K., Tubić, A., Šolić, M., Kordić, B., et al. (2021). Synthesis, characterization and application of magnetic nanoparticles modified with Fe-Mn binary oxide for enhanced removal of As(III) and As(V). *Environ. Technol.* 42, 2527–2539. doi:10.1080/09593330.2019.1705919

Otero-González, L., Mikhalovsky, S. V., Václavíková, M., Trenikhin, M. V., Cundy, A. B., and Savina, I. N. (2020). Novel nanostructured iron oxide cryogels for arsenic (As (III)) removal. *J. Hazard. Mater.* 381, 120996. doi:10.1016/j.jhazmat.2019.120996

Pardo, A., Pelaz, B., del Pino, P., Al-Modlej, A., Cambón, A., Velasco, B., et al. (2021). Monodisperse superparamagnetic nanoparticles separation adsorbents for high-yield removal of arsenic and/or mercury metals in aqueous media. *J. Mol. Liq.* 335, 116485. doi:10.1016/j.molliq.2021.116485

Paul, B., Parashar, V., and Mishra, A. (2015). Graphene in the Fe_3O_4 nanocomposite switching the negative influence of humic acid coating into an enhancing effect in the removal of arsenic from water. *Environ. Sci. Water Res. Technol.* 1, 77–83. doi:10.1039/c4ew00034j

Peng, Y., Azeem, M., Li, R., Xing, L., Li, Y., Zhang, Y., et al. (2022). Zirconium hydroxide nanoparticle encapsulated magnetic biochar composite derived from rice residue: Application for As(III) and As(V) polluted water purification. *J. Hazard. Mat.* 423, 127081. doi:10.1016/j.jhazmat.2021.127081

Pholosi, A., Naidoo, E. B., and Ofomaja, A. E. (2019). Enhanced Arsenic (III) adsorption from aqueous solution by magnetic pine cone biomass. *Mat. Chem. Phys.* 222, 20–30. doi:10.1016/j.matchemphys.2018.09.067

Powell, C. D., Atkinson, A. J., Ma, Y., Marcos-Hernandez, M., Villagran, D., Westerhoff, P., et al. (2020). Magnetic nanoparticle recovery device (MagNERD) enables application of iron oxide nanoparticles for water treatment. *J. Nanoparticle Res.* 22, 48–11. doi:10.1007/s11051-020-4770-4

Qi, B., Hu, X., Cui, S., Liu, H., Li, Y., Li, Y., et al. (2023). Rapid fabrication of superhydrophobic magnetic melt-blown fiber felt for oil spill recovery and efficient oil–water separation. *Sep. Purif. Technol.* 306, 122486. doi:10.1016/j.seppur.2022.122486

Qi, J., Zhang, G., and Li, H. (2015). Efficient removal of arsenic from water using a granular adsorbent: Fe-Mn binary oxide impregnated chitosan bead. *Bioresour. Technol.* 193, 243–249. doi:10.1016/j.biortech.2015.06.102

Qi, P., Luo, R., Pichler, T., Zeng, J., Wang, Y., Fan, Y., et al. (2019). Development of a magnetic core-shell Fe_3O_4@TA@UiO-66 microsphere for removal of arsenic(III) and antimony(III) from aqueous solution. *J. Hazard. Mat.* 378, 120721. doi:10.1016/j.jhazmat.2019.05.114

Rahaman, M. S., Rahman, M. M., Mise, N., Sikder, M. T., Ichihara, G., Uddin, M. K., et al. (2021). Environmental arsenic exposure and its contribution to human diseases, toxicity mechanism and management. *Environ. Pollut.* 289, 117940. doi:10.1016/j.envpol.2021.117940

Rajesh Kumar, S., Jayavignesh, V., Selvakumar, R., Swaminathan, K., and Ponpandian, N. (2016). Facile synthesis of yeast cross-linked Fe_3O_4nanoadsorbents for efficient removal of aquatic environment contaminated with As(V). *J. Colloid Interface Sci.* 484, 183–195. doi:10.1016/j.jcis.2016.08.081

Rao, P., Sun, Z., Zhang, W., Yao, W., Wang, L., and Ding, G. (2015). Preparation and application of amorphous Fe-Ti bimetal oxides for arsenic removal. *RSC Adv.* 5, 89545–89551. doi:10.1039/c5ra12039j

Ren, Z., Zhang, G., and Paul Chen, J. (2011). Adsorptive removal of arsenic from water by an iron-zirconium binary oxide adsorbent. *J. Colloid Interface Sci.* 358, 230–237. doi:10.1016/j.jcis.2011.01.013

Rowley, J., and Abu-Zahra, N. H. (2019). Synthesis and characterization of polyethersulfone membranes impregnated with (3-aminopropyltriethoxysilane) APTES-Fe_3O_4 nanoparticles for As(V) removal from water. *J. Environ. Chem. Eng.* 7, 102875. doi:10.1016/j.jece.2018.102875

Sahu, U. K., Sahu, M. K., Mohapatra, S. S., and Patel, R. K. (2016). Removal of As(V) from aqueous solution by Ce-Fe bimetal mixed oxide. *J. Environ. Chem. Eng.* 4, 2892–2899. doi:10.1016/j.jece.2016.05.041

Sakthivel, T. S., Das, S., Pratt, C. J., and Seal, S. (2017). One-pot synthesis of a ceria–graphene oxide composite for the efficient removal of arsenic species. *Nanoscale* 9, 3367–3374. doi:10.1039/c6nr07608d

Scaria, J., Nidheesh, P. V., and Kumar, M. S. (2020). Synthesis and applications of various bimetallic nanomaterials in water and wastewater treatment. *J. Environ. Manage.* 259, 110011. doi:10.1016/j.jenvman.2019.110011

Selvaraj, R., Pai, S., Vinayagam, R., Varadavenkatesan, T., Kumar, P. S., Duc, P. A., et al. (2022). A recent update on green synthesized iron and iron oxide nanoparticles for environmental applications. *Chemosphere* 308, 136331. doi:10.1016/j.chemosphere.2022.136331

Sha, T., Hu, W., Dong, J., Chi, Z., Zhao, Y., and Huang, H. (2020). Influence of the structure and composition of Fe–Mn binary oxides on rGO on As(III) removal from aquifers. *J. Environ. Sci. (China)* 88, 133–144. doi:10.1016/j.jes.2019.08.008

Shaji, E., Santosh, M., Sarath, K. V., Prakash, P., Deepchand, V., and Divya, B. V. (2021). Arsenic contamination of groundwater: A global synopsis with focus on the Indian peninsula. *Geosci. Front.* 12, 101079. doi:10.1016/j.gsf.2020.08.015

Shan, C., and Tong, M. (2013). Efficient removal of trace arsenite through oxidation and adsorption by magnetic nanoparticles modified with Fe-Mn binary oxide. *Water Res.* 47, 3411–3421. doi:10.1016/j.watres.2013.03.035

Shokoohi, R., Khazaei, M., Karami, M., Seidmohammadi, A., Berijani, N., Khotanlou, H., et al. (2021). The relationship between chronic exposure to arsenic through drinking water and hearing function in exposed population aged 10–49 years: A cross-sectional study. *Ecotoxicol. Environ. Saf.* 211, 111939. doi:10.1016/j.ecoenv.2021.111939

Siddiqui, S. I., and Chaudhry, S. A. (2019). Nanohybrid composite Fe_2O_3 -ZrO_2/BC for inhibiting the growth of bacteria and adsorptive removal of arsenic and dyes from water. *J. Clean. Prod.* 223, 849–868. doi:10.1016/j.jclepro.2019.03.161

Simeonidis, K., Mourdikoudis, S., Kaprara, E., Mitrakas, M., and Polavarapu, L. (2016). Inorganic engineered nanoparticles in drinking water treatment: A critical review. *Environ. Sci. Water Res. Technol.* 2, 43–70. doi:10.1039/c5ew00152h

Singh, P., Sarswat, A., Pittman, C. U., Mlsna, T., and Mohan, D. (2020). Sustainable low-concentration arsenite [as(III)] removal in single and multicomponent systems using hybrid iron oxide-biochar nanocomposite adsorbents - a mechanistic study. *ACS Omega* 5, 2575–2593. doi:10.1021/acsomega.9b02842

Singh, R., Gayen, A., Kumar, S., and Dewangan, R. (2021). Geo-spatial distribution of arsenic contamination of groundwater resources in intricate crystalline aquifer system of Central India: Arsenic toxicity manifestation and health risk assessment. *Hum. Ecol. Risk Assess.* 27, 1588–1612. doi:10.1080/10807039.2020.1865787

Smedley, P. L., and Kinniburgh, D. G. (2002). A review of the source, behaviour and distribution of arsenic in natural waters. *Appl. Geochem.* 17, 517–568. doi:10.1016/s0883-2927(02)00018-5

Stumm, W. (1992). *Chemistry of the solid-water interface: Processes at the mineral-water and particle-water interface in natural systems.* Hoboken, NJ: Wiley-Interscience, 397.

Su, H., Ye, Z., and Hmidi, N. (2017a). High-performance iron oxide–graphene oxide nanocomposite adsorbents for arsenic removal. *Colloids Surfaces APhysicochem. Eng. Asp.* 522, 161–172. doi:10.1016/j.colsurfa.2017.02.065

Su, H., Ye, Z., Hmidi, N., and Subramanian, R. (2017b). Carbon nanosphere-iron oxide nanocomposites as high-capacity adsorbents for arsenic removal. *RSC Adv.* 7, 36138–36148. doi:10.1039/c7ra06187k

Torasso, N., Vergara-Rubio, A., Rivas-Rojas, P., Huck-Iriart, C., Larrañaga, A., Fernández-Cirelli, A., et al. (2021). Enhancing arsenic adsorption via excellent dispersion of iron oxide nanoparticles inside poly(vinyl alcohol) nanofibers. *J. Environ. Chem. Eng.* 9, 104664. doi:10.1016/j.jece.2020.104664

Tripathy, M., Padhiari, S., and Hota, G. (2020). L-Cysteine-Functionalized mesoporous magnetite nanospheres: Synthesis and adsorptive application toward arsenic remediation. *J. Chem. Eng. Data.* 65, 3906–3919. doi:10.1021/acs.jced.0c00250

Tyler, C. R., and Allan, A. M. (2014). The effects of arsenic exposure on neurological and cognitive dysfunction in human and rodent studies: A review. *Curr. Environ. Heal. Rep.* 1, 132–147. doi:10.1007/s40572-014-0012-1

Usman, M., Byrne, J. M., Chaudhary, A., Orsetti, S., Hanna, K., Ruby, C., et al. (2018). Magnetite and green rust: Synthesis, properties, and environmental applications of mixed-valent iron minerals. *Chem. Rev.* 118, 3251–3304. doi:10.1021/acs.chemrev.7b00224

Vences-Alvarez, E., Lopez-Valdivieso, A., Cházaro-Ruíz, L. F., Flores-Zuñiga, H., and Rangel-Mendez, J. R. (2020). Enhanced arsenic removal from water by a bimetallic material ZrOx-FeOx with high OH density. *Environ. Sci. Pollut. Res.* 27, 33362–33372. doi:10.1007/s11356-020-09492-8

Wang, H., Yang, Q., Ma, H., and Liang, J. (2021). Chemical compositions evolution of groundwater and its pollution characterization due to agricultural activities in Yinchuan Plain, northwest China. *Environ. Res.* 200, 111449. doi:10.1016/j.envres.2021.111449

Wang, L., Shi, C., Pan, L., Zhang, X., and Zou, J. J. (2020). Rational design, synthesis, adsorption principles and applications of metal oxide adsorbents: A review. *Nanoscale* 12, 4790–4815. doi:10.1039/c9nr09274a

Wang, L., Wang, J. M., Zhang, R., Liu, X. G., Song, G. X., Chen, X. F., et al. (2016). Highly efficient As(v)/Sb(v) removal by magnetic sludge composite: Synthesis, characterization, equilibrium, and mechanism studies. *RSC Adv.* 6, 42876–42884. doi:10.1039/c6ra06208c

Wen, Z., Dai, C., Zhu, Y., and Zhang, Y. (2015a). Arsenate removal from aqueous solutions using magnetic mesoporous iron manganese bimetal oxides. *RSC Adv.* 5, 4058–4068. doi:10.1039/c4ra09746g

Wen, Z., Lu, J., Zhang, Y., Cheng, G., Huang, S., Chen, J., et al. (2020). Facile inverse micelle fabrication of magnetic ordered mesoporous iron cerium bimetal oxides with excellent performance for arsenic removal from water. *J. Hazard. Mat.* 383, 121172. doi:10.1016/j.jhazmat.2019.121172

Wen, Z., Zhang, Y., Cheng, G., Wang, Y., and Chen, R. (2019). Simultaneous removal of As(V)/Cr(VI) and acid orange 7 (AO7) by nanosized ordered magnetic mesoporous Fe-Ce bimetal oxides: Behavior and mechanism. *Chemosphere* 218, 1002–1013. doi:10.1016/j.chemosphere.2018.11.208

Wen, Z., Zhang, Y., Dai, C., and Sun, Z. (2015b). Nanocasted synthesis of magnetic mesoporous iron cerium bimetal oxides (MMIC) as an efficient heterogeneous Fenton-like catalyst for oxidation of arsenite. *J. Hazard. Mat.* 287, 225–233. doi:10.1016/j.jhazmat.2015.01.065

Wu, H., Yin, J. J., Wamer, W. G., Zeng, M., and Lo, Y. M. (2014). Reactive oxygen species-related activities of nano-iron metal and nano-iron oxides. *J. Food Drug Anal.* 22, 86–94. doi:10.1016/j.jfda.2014.01.007

Xu, W., Yang, T., Liu, S., Du, L., Chen, Q., Li, X., et al. (2022). Insights into the Synthesis, types and application of iron Nanoparticles: The overlooked significance of environmental effects. *Environ. Int.* 158, 106980. doi:10.1016/j.envint.2021.106980

Yadav, V. K., Ali, D., Khan, S. H., Gnanamoorthy, G., Choudhary, N., Yadav, K. K., et al. (2020a). Synthesis and characterization of amorphous iron oxide nanoparticles by the sonochemical method and their application for the remediation of heavy metals from wastewater. *Nanomaterials* 10 (8), 1551. doi:10.3390/nano10081551

Yadav, V. K., Yadav, K. K., Gnanamoorthy, G., Choudhary, N., Khan, S. H., Gupta, N., et al. (2020b). A novel synthesis and characterization of polyhedral shaped amorphous iron oxide nanoparticles from incense sticks ash waste. *Environ. Technol. Innovation* 20, 101089. doi:10.1016/j.eti.2020.101089

Yavuz, C. T., Mayo, J. T., Yu, W. W., Prakash, A., Falkner, J. C., Yean, S., et al. (2006). Low-field magnetic separation of monodisperse Fe_3O_4 nanocrystals. *Science* 314, 964–967. doi:10.1126/science.1131475

Yu, L., Liu, H., Liu, C., Lan, H., and Qu, J. (2016). Magnetically-confined Fe-Mn bimetallic oxide encapsulation as an efficient and recoverable adsorbent for arsenic(III) removal. *Part. Part. Syst. Charact.* 33, 323–331. doi:10.1002/ppsc.201600009

Yu, L., Yu, Y., Li, J., and Chen, J. P. (2019). Development and characterization of yttrium-ferric binary composite for treatment of highly concentrated arsenate wastewater. *J. Hazard. Mat.* 361, 348–356. doi:10.1016/j.jhazmat.2018.07.068

Yu, Y., Yu, L., Shih, K., and Chen, J. P. (2018). Yttrium-doped iron oxide magnetic adsorbent for enhancement in arsenic removal and ease in separation after applications. *J. Colloid Interface Sci.* 521, 252–260. doi:10.1016/j.jcis.2018.02.046

Zamora-Ledezma, C., Negrete-Bolagay, D., Figueroa, F., Zamora-Ledezma, E., Ni, M., Alexis, F., et al. (2021). Heavy metal water pollution: A fresh look about hazards, novel and conventional remediation methods. *Environ. Technol. Innov.* 22, 101504. doi:10.1016/j.eti.2021.101504

Zhang, G., Liu, F., Liu, H., Qu, J., and Liu, R. (2014). Respective role of Fe and Mn oxide contents for arsenic sorption in iron and manganese binary oxide: An X-ray absorption spectroscopy investigation. *Environ. Sci. Technol.* 48, 10316–10322. doi:10.1021/es501527c

Zhang, G., Ren, Z., Zhang, X., and Chen, J. (2013). Nanostructured iron(III)-copper(II) binary oxide: A novel adsorbent for enhanced arsenic removal from aqueous solutions. *Water Res.* 47, 4022–4031. doi:10.1016/j.watres.2012.11.059

Zhang, G., Xu, X., Ji, Q., Liu, R., Liu, H., Qu, J., et al. (2017). Porous nanobimetallic Fe-Mn cubes with high valent Mn and highly efficient removal of arsenic(III). *ACS Appl. Mat. Interfaces* 9, 14868–14877. doi:10.1021/acsami.7b02127

Zhang, M., Ma, X., Li, J., Huang, R., Guo, L., Zhang, X., et al. (2019). Enhanced removal of As(III) and As(V) from aqueous solution using ionic liquid-modified magnetic graphene oxide. *Chemosphere* 234, 196–203. doi:10.1016/j.chemosphere.2019.06.057

Zhang, S., Niu, H., Cai, Y., Zhao, X., and Shi, Y. (2010). Arsenite and arsenate adsorption on coprecipitated bimetal oxide magnetic nanomaterials: $MnFe_2O_4$ and $CoFe_2O_4$. *Chem. Eng. J.* 158, 599–607. doi:10.1016/j.cej.2010.02.013

Zhao, G., Huang, X., Tang, Z., Huang, Q., Niu, F., and Wang, X. (2018). Polymer-based nanocomposites for heavy metal ions removal from aqueous solution: A review. *Polym. Chem.* 9, 3562–3582. doi:10.1039/c8py00484f

Nomenclature

Parameters (Nomenclature) Unit

Average size of nanoparticles (PS) in nm
Surface area of nanoparticles (S) in $m^2\ g^{-1}$
Average pore size of adsorbent (D) in nm
Lamellar thickness (d_L) in nm
Membrane thickness (d_M) in μm
Mass surface density (rA) mg cm^{-2}
Pore volume of the adsorbent (V_p) in $cm^3\ g^{-1}$
The saturation magnetization of adsorbent (M_s) in emu g^{-1}
Point Zero Charge of adsorbent (pH_{PZC})
Isoelectric point (IEP)
Contaminant arsenic species As(III), As(V)
Initial arsenic concentration [As(III)] and [As(V)] in mg L^{-1}
Adsorbent dose [Ads] in gL^{-1}
Temperature (T) in °C
Equilibrium time (t_{eq}) in Hour (h)
Efficiency (η) in %
Reduction of removal efficiency (Δη) in %
Maximum adsorption capacity (q_m) in mg g^{-1}
Desorption efficiency (γ) in %
Arsenic recovery ratio (R) in %
Number of regeneration cycles (RC)
Residual efficiency after regeneration (η_R) in %
Pseudo-First-order (PFO)
Pseudo-Second-order (PSO)
Second-order (SO)
Langmuir isotherm model (LIM)
Freundlich isotherm model (FIM)
Redlich-Peterson isotherm model (RPI)
Transmission electron microscopy (TEM)
X-ray photoelectron spectroscopy (XPS)
Reactive oxygen species (ROS)